Monthly Notices
of the
ROYAL ASTRONOMICAL SOCIETY

MNRAS **433,** 2764–2789 (2013) doi:10.1093/mnras/stt890
Advance Access publication 2013 June 29

Galaxy And Mass Assembly: evolution of the Hα luminosity function and star formation rate density up to $z < 0.35$

M. L. P. Gunawardhana,[1,2⋆] A. M. Hopkins,[2⋆] J. Bland-Hawthorn,[1] S. Brough,[2] R. Sharp,[3] J. Loveday,[4] E. Taylor,[1,5] D. H. Jones,[6] M. A. Lara-López,[2] A. E. Bauer,[2] M. Colless,[2,3] M. Owers,[2] I. K. Baldry,[7] A. R. López–Sánchez,[2,8] C. Foster,[9] S. Bamford,[10] M. J. I. Brown,[5] S. P. Driver,[11,12] M. J. Drinkwater,[13] J. Liske,[9] M. Meyer,[11] P. Norberg,[14] A. S. G. Robotham,[11] J. H. Y. Ching,[1] M. E. Cluver,[2] S. Croom,[1] L. Kelvin,[11,12] M. Prescott,[15] O. Steele,[16] D. Thomas[16] and L. Wang[14]

[1]*Sydney Institute for Astronomy (SIfA), School of Physics, University of Sydney, NSW 2006, Australia*
[2]*Australian Astronomical Observatory, PO Box 915, North Ryde, NSW 1670, Australia*
[3]*Research School of Astronomy & Astrophysics, Australian National University, Cotter Road, Weston Creek, ACT 2611, Australia*
[4]*Astronomy Centre, University of Sussex, Falmer, Brighton BN1 9QH, UK*
[5]*School of Physics, The University of Melbourne, Parkville, VIC 3010, Australia*
[6]*School of Physics, Monash University, Clayton, Victoria 3800, Australia*
[7]*Astrophysics Research Institute, Liverpool John Moores University, Twelve Quays House, Egerton Wharf, Birkenhead CH41 1LD, UK*
[8]*Department of Physics and Astronomy, Macquarie University, NSW 2109, Australia*
[9]*European Southern Observatory, Karl-Schwarzschild-Str 2, D-85748 Garching, Germany*
[10]*School of Physics & Astronomy, University of Nottingham, University Park, Nottingham NG7 2RD, UK*
[11]*International Centre for Radio Astronomy Research (ICRAR), University of Western Australia, Crawley, WA 6009, Australia*
[12]*Scottish Universities' Physics Alliance (SUPA), School of Physics and Astronomy, University of St Andrews, North Haugh, St Andrews KY16 9SS, UK*
[13]*School of Mathematics and Physics, University of Queensland, QLD 4072, Australia*
[14]*Institute for Computational Cosmology, Department of Physics, Durham University, South Road, Durham DH1 3LE, UK*
[15]*Department of Physics, University of the Western Cape, Private Bag X17, Bellville 7535, South Africa*
[16]*Institute of Cosmology and Gravitation, University of Portsmouth, Dennis Sciama Building, Portsmouth PO1 3FX, UK*

Accepted 2013 May 20. Received 2013 May 17; in original form 2012 July 15

ABSTRACT

Measurements of the low-z Hα luminosity function, Φ, have a large dispersion in the local number density of sources ($\sim$0.5–1 Mpc^{-3} dex^{-1}), and correspondingly in the star formation rate density (SFRD). The possible causes for these discrepancies include limited volume sampling, biases arising from survey sample selection, different methods of correcting for dust obscuration and active galactic nucleus contamination. The Galaxy And Mass Assembly (GAMA) survey and Sloan Digital Sky Survey (SDSS) provide deep spectroscopic observations over a wide sky area enabling detection of a large sample of star-forming galaxies spanning $0.001 < \mathrm{SFR}_{\mathrm{H}\alpha}$ ($\mathrm{M}_{\odot}$ yr^{-1}) < 100 with which to robustly measure the evolution of the SFRD in the low-z Universe. The large number of high-SFR galaxies present in our sample allow an improved measurement of the bright end of the luminosity function, indicating that the decrease in Φ at bright luminosities is best described by a Saunders functional form rather than the traditional Schechter function. This result is consistent with other published luminosity functions in the far-infrared and radio. For GAMA and SDSS, we find the r-band apparent magnitude limit, combined with the subsequent requirement for Hα detection leads to an incompleteness due to missing bright Hα sources with faint r-band magnitudes.

Key words: surveys – galaxies: evolution – galaxies: formation – galaxies: interactions – galaxies: luminosity function, mass function – galaxies: starburst.

⋆ E-mail: m.gunawardhana@physics.usyd.edu.au (MLPG); ahopkins@aao.gov.au (AMH)

1 INTRODUCTION

The evolution of the global star formation rate density (SFRD) is now traced out to $z \sim 10$ using star formation indicators across a broad wavelength range, from X-ray/gamma rays to radio emission. Direct information on the SFR has been collected from nebular emission lines such as [O II] λ3727, [O III] λ5007, Hα, Hβ (Glazebrook et al. 2004; Westra et al. 2010, and references therein) tracing massive stars, ultraviolet, far- and mid-infrared emission (Pérez-González et al. 2005; Schiminovich et al. 2005; Reddy et al. 2007; Reddy & Steidel 2009; Bouwens et al. 2010, 2011; López-Sánchez 2010) revealing young star-forming regions, radio emission produced in supernova remnants (Haarsma et al. 2000; Seymour et al. 2008), X-ray emission produced from high-mass X-ray binaries (Georgakakis et al. 2003; Fabbiano 2005) and gamma-ray bursts produced from massive stellar explosions (Woosley & Bloom 2006; Yüksel et al. 2008; Kistler et al. 2009).

The cosmic star formation history (SFH) indicates a global increase in star formation activity since the formation of the first galaxies, reaching a peak at $z \sim 2$–3. This is followed by a rapid decline in average star formation of approximately a factor of 10 (e.g. Lilly et al. 1996; Madau et al. 1996; Hopkins 2004; Hopkins & Beacom 2006; Pérez-González et al. 2008). This is typically interpreted in the model of mass dependence (Cowie, Songaila & Barger 1999), which states that high-mass galaxies formed their stars early and rapidly, with lower mass systems forming more slowly and at later times. Evidence supporting this idea in the context of the mass dependence of the SFH has accumulated over recent years (e.g. Feulner et al. 2005; Juneau et al. 2005; Zheng et al. 2007; Mobasher et al. 2009).

Numerous studies have been conducted to determine the physical processes contributing to the shape of the cosmic SFH, particularly the substantial decline in star formation activity since $z \sim 2$. Hydrodynamic simulations examining hot and cold mode accretion indicate a close relationship between the global gas infall rate and the cosmic SFR (Kereš et al. 2005; van de Voort et al. 2011). A mechanism associated directly with star formation itself has been proposed that moderates the relation between neutral gas and SFR in galaxies (Hopkins, McClure-Griffiths & Gaensler 2008). Through the analysis of rest-frame u-band luminosities, Prescott, Baldry & James (2009) find evidence of a decline in characteristic luminosity (L^*) over $0 < z < 1.2$, coinciding with the decline in global star formation. A change in the rate and mode of star formation since $z \sim 1$ is assumed to be responsible for this. The strong decrease in the fraction of galaxies undergoing starbursts (Dressler et al. 2009) and the decline in galaxy interactions such as tidal encounters and mergers (Le Fèvre et al. 2000; De Propris et al. 2007; Lotz et al. 2008, 2011) are given as possible explanations. Recent work (Nakamura et al. 2004; Sobral et al. 2009; López-Sánchez 2010; Westra et al. 2010) points out a link between star formation and galaxy morphology, indicating that the merger-induced star formation tends to dominate in galaxies with $L > L^*$, with a more quiescent mode dominating in fainter galaxies.

While the SFH based on different SFR tracers gives a broadly consistent picture of the evolution of the global star formation, the dispersion between individual measurements at a given redshift is striking and can span more than 0.5 dex (e.g. Hopkins & Beacom 2006). Ideally, studying the cosmic SFH using SFR indicators covering a large spectral range would provide a robustly consistent picture of galaxy formation and evolution. In reality, different SFR indicators suffer from different selection and calibration biases (e.g. the sensitivity to the stellar metallicity abundance and the ionization state in the case of [O II] λ3727), and are affected by and treated for dust obscuration differently (Gilbank et al. 2010; Wijesinghe et al. 2011), introducing systematic uncertainties to measurements. Hα emission, as a direct tracer of instantaneous star formation in a galaxy, is a good candidate for providing an accurate view of the evolution of SFRD. It is, however, currently restricted to low-to-moderate redshift, and even with the use of a common SFR indicator, a compilation of local Hα SFRDs (Sobral et al. 2009; Westra et al. 2010) still shows large discrepancies between measurements. The possible causes for this dispersion include cosmic (sample) variance, the differences in selection criteria between surveys, and the uncertainties coming from the measurements, corrections and assumptions that go into the final estimate of SFRDs. We aim to understand and interpret the observed evolution of cosmic SFRD paying special attention to the advantages, and drawbacks of survey and sample selection.

An additional complication is that different SFR indicators probe different stellar mass ranges (e.g. Hα emission traces stars with masses $\geq$10 $M_\odot$). In order to infer an SFRD therefore requires the assumption of a stellar initial mass function (IMF). The stellar IMF is widely accepted to have a universal form regardless of environment and time (e.g. Bastian, Covey & Meyer 2010). There are a number of recent studies, however, that suggest variations in the stellar IMF with respect to redshift (Chary 2008; Wilkins et al. 2008a,b; Davé 2011), surface brightness (Hoversten & Glazebrook 2008; Meurer et al. 2009) and SFR or SFR surface density (Gunawardhana et al. 2011) or colour (Dutton et al. 2011). An environment-dependent and/or evolving IMF directly impacts the derived cosmic SFRDs. Although not explicitly explored in this paper, the incorporation of such an IMF can be a potential solution towards reconciling the observed discrepancies in the evolution of the cosmic SFR and stellar mass densities (Wilkins et al. 2008a).

Many local SFRDs come from narrow-band filter surveys (e.g. Jones & Bland-Hawthorn 2001; Pascual et al. 2001; Fujita et al. 2003; Glazebrook et al. 2004; Ly et al. 2007, 2011; Dale et al. 2008; Shioya et al. 2008) complementing those from spectroscopic surveys (e.g. Tresse & Maddox 1998; Sullivan et al. 2000; Tresse et al. 2002; Pérez-González et al. 2003; Shim et al. 2009; Gilbank et al. 2010; Westra et al. 2010). In contrast to spectroscopic surveys, narrow-band surveys at optical wavelengths provide deep imaging over a narrow-redshift slice, yielding relatively large volume-limited samples of galaxies. Also, the target selection is done through emission lines. The two main advantages with narrow-band surveys are that they are most effective at detecting faint emission-line sources, and the galaxies are selected using a quantity they aim to measure, which scales with SFR (Jones & Bland-Hawthorn 2001; Westra & Jones 2008).

There are, however, a number of drawbacks to narrow-band surveys. The main disadvantages are the need to assume common corrections for stellar absorption, dust obscuration, contamination by active galactic nucleus (AGN) and insensitivity to low equivalent widths (EWs). These assumptions introduce large uncertainties and can lead to a systematic underestimate of the final SFRD (Massarotti, Iovino & Buzzoni 2001; James et al. 2004; Spector, Finkelman & Brosch 2012). In contrast, spectroscopy allows the determination of such corrections individually for each galaxy. Moreover, a survey with a large sky coverage is generally preferred in order to overcome cosmic (sample) variance and small number statistics. Despite being deep, the current generation of narrow-band surveys only cover a relatively limited sky area. Even for spectroscopic surveys, only the Sloan Digital Sky Survey (SDSS): Stripe

82 (Gilbank et al. 2010, area ∼275 deg^2 and $z \lesssim 0.2$[1]) Universidad Complutense de Madrid (UCM) survey (Gallego et al. 1995; Pérez-González et al. 2003, area ∼472 deg^2 and $z \lesssim 0.045$) and now the Galaxy And Mass Assembly (GAMA[2]) survey (Driver et al. 2009, 2011, area ∼144 deg^2 and $z \lesssim 0.35$) provide substantial sky coverage.

The layout of this paper is as follows. We describe sample selection in Section 2 and provide a brief introduction to the GAMA and SDSS surveys. Section 3 details the derivation of physical properties such as Hα SFRs for the two samples. In Section 4, we describe the technical details of the derivation of the luminosity functions (LFs), taking into account different survey selection criteria. This section also presents the resulting GAMA and SDSS LFs. Section 5 describes the details of the functional types used to fit the LFs. In Section 6, we infer SFRDs for our GAMA and SDSS LFs, and in the Appendix A we explore the potential biases influencing our estimates of SFRDs.

The assumed cosmological parameters are $H_0 = 70$ km s^{-1} Mpc^{-1}, $\Omega_M = 0.3$ and $\Omega_\Lambda = 0.7$. All magnitudes are presented in the AB system.

2 DATA

In this study, we utilize the GAMA phase-I survey, which covers three equatorial fields of 48 deg^2 each, with two fields reaching a depth of $r_{AB} < 19.4$ mag and the third extending to $r_{AB} < 19.8$ mag. There are ∼136 000 galaxies with measured spectra available from GAMA observations (Driver et al. 2009, 2011). The availability of such a large galaxy sample with deep spectroscopic observations (∼2 mag fainter than SDSS) over a wide sky area, covering a modest redshift range allows the determination of the evolution of the SFH in the local universe in a consistent manner with reduced systematic and sampling biases.

We also use the SDSS Data Release 7 (DR7) spectroscopic galaxy sample (Abazajian et al. 2009) in this study. SDSS-DR7 covers an sky area of >8000 deg^2, with $0 < z < 0.38$ and $r_{AB} < 17.77$, providing the largest galaxy sample to date.

2.1 GAMA survey and data

GAMA is a spectroscopic survey undertaken at the Anglo-Australian Telescope (AAT). GAMA spectroscopic targets were selected from the SDSS Data Release 6 (Adelman-McCarthy et al. 2008) to limiting Petrosian magnitudes of $r < 19.4$ in two fields, and $r < 19.8$ in the third field. Baldry et al. (2010) provides a detailed discussion of the GAMA input catalogue, and the tiling of the sources is described in Robotham et al. (2010).

For this paper, we use GAMA I data consisting of GAMA, SDSS, 2-degree field Galaxy Redshift Survey (2dFGRS) and Millennium Galaxy Catalogue (MGC) sources. The GAMA spectra are obtained from the AAT with the 2-degree Field (2dF) fibre feed and AAOmega multi-object spectrograph. AAOmega provides a resolution of 3.2 Å full width at half-maximum (FWHM) with complete spectral coverage from 3700 to 8900 Å (Sharp et al. 2006; Driver et al. 2011). The spectra are sky subtracted following Sharp & Parkinson (2010), and redshifts are assigned with RUNZ (Saunders, Cannon & Sutherland 2004), a FORTRAN program for measuring redshifts from reduced spectra. Spectra were given a redshift quality (nQ), with nQ > 2 regarded as a secure redshift (Driver et al. 2011). GAMA does not re-observe the majority of SDSS, 2dFGRS and MGC galaxies in the three GAMA regions.

GAMA I spectroscopic data set is over 98 per cent complete in spectroscopic follow-up (Driver et al. 2011), the small spectroscopic incompleteness likely due to low-luminosity, low surface-brightness galaxies. In addition, GAMA, like all spectroscopic surveys, suffers from several other sources of incompleteness: imaging incompleteness and redshift measurement failures, i.e. spectra with nQ ≤ 2 (Loveday et al. 2012). The LFs presented in this paper are corrected for these sources of incompleteness, see Section 4 and Section A1.2.

All GAMA spectra are flux calibrated following the detailed discussion given in Hopkins et al. (2013) and Liske et al. (in preparation). Briefly, the GAMA flux calibration process is essentially a two-step process. In the first instance, an initial flux calibration is achieved for each 2dF plate to correct for the wavelength dependence of the system throughput. This is then supplemented by an absolute flux correction.

Three fibres on each 2dF plate are assigned to standard stars. For each star a flux-correction vector is derived by taking the ratio of the observed to its best-fitting model, the average between the three provides a unique wavelength-dependent correction for a given plate. Any lower order shape in the continuum is removed by dividing the standard stellar spectrum by the unique correction vector. A fit to the residuals achieves an initial curvature correction that accounts for the poor CCD response at blue and red extremes of the spectrum. An absolute flux calibration is obtained by tying the spectrophotometry directly to the *r*-band Petrosian magnitudes from the SDSS photometry.

The standard strong optical emission lines are measured from each curvature-corrected and flux-calibrated spectrum assuming a single Gaussian approximation and a common redshift and line-width within an adjacent set of lines (e.g. Hα and the [N II] $\lambda\lambda$6548, 6583 doublet), and simultaneously fitting the continuum local to the set of lines (Brough et al. 2011; Hopkins et al. 2013). Corrections for the underlying Balmer stellar absorption, dust obscuration and fibre aperture effects, detailed below, are applied to these measurements. The GAMA sample consists of a relatively large number of low-z galaxies. The observed recessional velocities of the nearest galaxies ($z < 0.02$) are influenced by peculiar motions. For these objects, the redshift distances will be systematically under- or overestimated if peculiar velocities are ignored. Parametric multi-attractor models provide directional-dependent prescriptions to estimate the effects of peculiar velocities. For this sample, the flow corrections have been made using the approach of Tonry et al. (2000), as described in Baldry et al. (2012). The derived physical properties of galaxies, such as luminosities, are based on these flow-corrected redshifts (DistancesFramesv06).

SDSS photometry in *u,g,r,i,z* filters is available for each GAMA galaxy. The intrinsic galaxy luminosities are measured in *r*-band-defined elliptical Kron apertures (Hill et al. 2011; Taylor et al. 2011). *k*-corrections to $z = 0$ (KCORRECT v4_2; Blanton & Roweis 2007) are applied and all photometry is corrected for foreground (Milky Way) dust extinction (Schlegel, Finkbeiner & Davis 1998).

2.1.1 *This sample*

Our sample is drawn from the 136 000 spectra (AATSpecAllv08) available in 2011 December, and is comprised of 72 880 galaxies with GAMA redshifts, measured Hα emission, nQ > 2 and Hα

[1] Redshift ranges given here do not necessarily denote the redshift coverage of the survey, but rather the redshift coverage corresponding to a particular emission line (e.g. Hα).

[2] http://www.gama-survey.org

Table 1. The total number of GAMA galaxies with Hα fluxes above the detection limit (i.e. 25×10^{-20} W m^{-2}) in four different redshift bins up to $z \sim 0.34$ and the approximate percentage of objects without measured BDs are given in the first part of the table. The SDSS galaxy numbers given are the SDSS galaxies in the three GAMA regions. Note that we have imposed a flux limit of 1×10^{-18} W m^{-2} (see Section 4.1.2) to construct the GAMA LFs presented in this paper. The second part of the table (the last two entries) indicates the total number of SDSS–DR7 galaxies with Hα fluxes above the flux limit (i.e. 1×10^{-18} W m^{-2}) in two different redshift bins up to $z \sim 0.2$ and the approximate percentage of objects without measured BDs.

z	Total No. of galaxies GAMA + SDSS in GAMA	No. from GAMA-9h	No. from GAMA-12h	No. from GAMA-15h	per cent without BDs	per cent with BD < 2.86
$0.001 < z < 0.1$	6928 + 3153	2936	4025	3120	4	24
$0.1 < z < 0.15$	10 700 + 2080	2714	5179	4887	9	16
$0.17 < z < 0.24$	13 287 + 462	4284	5618	3847	17	12
$0.24 < z < 0.34$	12 262 + 126	3384	5962	3042	18	9
z	Total No. of galaxies SDSS-DR7				per cent without BDs	per cent with BD < 2.86
$0.001 < z < 0.1$	140791	–	–	–	<0.1	2
$0.1 < z < 0.2$	70534	–	–	–	0.3	0.2

emission signal to noise (S/N) above 3. The Hα S/N is defined as the ratio of the observed Hα flux to the RMS noise over a 153 Å window 12 Å bluewards of the redshifted wavelength of the [N II] λ6548 feature. Furthermore, a selection of nQ = 2 sources obeying the constraints detailed in Baldry et al. (2012) are also included in the sample.

The redshift source of the brightest galaxies in GAMA is SDSS as GAMA does not re-observe most of these galaxies (Table 1). The emission-line measurements for the SDSS galaxies are from the MPA-JHU DR7 data base.[3] There are 11 675 SDSS sources with detected Hα emission included in the sample. The emission measurements for MGC sources are not currently available, and while the emission measurements for the 2dFGRS sources are available, the spectra from which these measures estimated are not flux calibrated. Therefore, these galaxies are excluded from our sample. The sample incompleteness introduced by the lack of 2dFGRS and MGC galaxies can be corrected for since the missing fractions are known (see Sections 4 A1.2).

Galaxies dominated by emission from AGNs are excluded from the sample based on standard optical emission-line ([N II] λ6584/Hα and [O III] λ5007/Hβ) diagnostics (Baldwin, Phillips & Terlevich-Baldwin et al. 1981, hereafter BPT) using the discrimination line of Kewley et al. (2001). In the case of galaxies for which only some of these four emission lines are measurable, AGNs can still be excluded using the diagnostics log([N II] λ6584/Hα) $\geq$ 0.2 and log([O III] λ5007/Hβ) $\geq$ 1. Overall $\sim$9 per cent of GAMA galaxies are classified as AGNs and excluded from our sample. For the galaxies still unable to be classified in this fashion, we flag them as 'unclassified', and retain them in the sample of star-forming galaxies. Of the star-forming sample, 30 per cent are 'unclassified' for this reason. We default to this solution rather than excluding them from the sample, as a galaxy with measured Hα but without an [N II] λ6584 or [O III] λ5007 measurement is more likely to be star forming than an AGN (Fernandes et al. 2010). Robotham et al. (2013) investigated the potential pitfalls of automated BPT classifications by visually examining a small sample of low-z GAMA galaxies. They found that the majority of the BPT classified AGNs are low-powered LINER-like systems with weak Hα, Hβ and [O III] λ5007. Furthermore, their results indicate that majority of the automated spectral classifications ($\sim$75 per cent) agree with the visual classifications. The impact of erroneously including a small fraction of AGNs is in any case very small, and does not change any of the conclusions below.

Furthermore, we exclude all galaxies with Hα emission measurements affected by the presence of strong sky lines, and all galaxies with Hα emission below a minimum flux limit of 25×10^{-20} W m^{-2}, hereafter called the detection limit. This detection limit is obtained from examining the spectra of a sample of low-Hα luminosity galaxies.

The GAMA emission-line sample spans $0 < z \leq 0.35$, and a large range in stellar mass ($7 \leq \log(M/M_{\odot}) \leq 12$; Taylor et al. 2011) and $0.001 \leq$ SFR ($M_{\odot}$ yr^{-1}) ≤ 100.

2.2 SDSS and DR7

In addition to the GAMA Hα LFs, we also construct the SDSS-DR7[4] (Abazajian et al. 2009) Hα LFs. SDSS (York et al. 2000) has imaged $\sim$10 000 deg^2 in five optical broad-band filters, using a wide-field imager with a mosaic CCD camera on a 2.5 m telescope, and covered the sky in a drift-scan mode in five filters (Gunn et al. 1998). Photometric catalogues are then used to identify the spectroscopic targets on the same telescope, using a 640-fibre-fed pair of multi-object double spectrographs. The wavelength coverage is from $\lambda\lambda$3800 to 9200 Å with a spectral resolution of $\lambda/\Delta\lambda \approx 2000$ (FWHM $\sim$ 2.4 Å at λ5000) (Abazajian et al. 2009). The SDSS-DR7 release presents the spectra for $\sim 10^6$ objects over a total sky area of 9380 deg^2. The main galaxy sample (MGC; Strauss et al. 2002) used in this study is complete to a Petrosian r-band magnitude limit of 17.77.

2.2.1 *This sample*

As for the SDSS sources in the GAMA fields, the emission-line measurements of the SDSS galaxies are from the MPA-JHU DR7 data base, and the derivation of these measurements is detailed in Brinchmann et al. (2004) and Tremonti et al. (2004). Briefly, each Galactic extinction-corrected galaxy spectrum is compared with a library of single stellar population models generated using the Bruzual & Charlot (2003) population synthesis code to fit the continuum shape. This accounts for weak features, and Balmer

[3] http://www.mpa-garching.mpg.de/SDSS/DR7/

[4] http://www.sdss.org/dr7/

stellar absorption. Once the best-fitting stellar population synthesis model to the continuum is subtracted and any remaining residuals are removed, Gaussian profiles are fitted simultaneously to all the emission lines, requiring that all the lines belonging to Balmer and forbidden-line series have the same width, and velocity offset. This requirement on line-widths, and velocity offsets, allow stronger/multiple lines to be used to constrain the weaker lines. The main difference between GAMA and SDSS emission-line samples is that the latter includes an implicit correction for stellar absorption effects. A constant correction for stellar absorption is incorporated when deriving Hα luminosities for GAMA galaxies (see Section 3). The assumption of a single value can introduce some uncertainty, and should be restricted to the examination of gross characteristics of large samples of galaxies (Hopkins et al. 2003), as is the case here. This assumption was shown by Gunawardhana et al. (2011) to have a minimal impact on all but the lowest SFR systems in the GAMA sample, and we explore this further in the context of the Hα LF in Section A1.1.

Similarly to GAMA, the redshifts of all the nearby galaxies in SDSS-DR7 are corrected for peculiar motions using Tonry et al. (2000). The photometric measurements are from the New York University value added catalogue (Blanton et al. 2005),[5] with *k*-corrections to $z = 0$ and the maximum redshift ($z_{\rm max}$) for each object derived using KCORRECT_v4_2 (Blanton & Roweis 2007) and the spectroscopic and flow-corrected redshifts of each object. Strictly speaking, heliocentric redshifts should be used in the estimation of *k*-corrections, although the difference in *k*-correction when using heliocentric or flow-corrected redshifts is negligible (Loveday et al. 2012). In summary, aside from the differences in emission-line and photometric measurements, other aspects such as the derivation of *k*-corrections and flow corrections are the same between the two samples.

The same flux selection in Hα used to select the GAMA star-forming sample is also applied to SDSS emission-line galaxies, and redshift warnings and standard flags given by the aforementioned data bases are used to remove artefacts/sources near stars. The final SDSS emission-line sample consists of 491 501 galaxies from which 14 per cent are classified as AGNs and excluded from our sample.

3 MEASURING LUMINOSITIES AND SFRs

3.1 Measuring Hα luminosities

As outlined in Gunawardhana et al. (2011) and Hopkins et al. (2003), measuring Hα luminosities, and SFRs, from fibre spectroscopy requires not only corrections for stellar absorption and obscuration, but also a correction for the aperture sampled by the fibre. Corrections for these effects are applied to all GAMA and SDSS galaxies as described below.

Following Hopkins et al. (2003), we derive an aperture, obscuration and Balmer stellar absorption corrected luminosity ($L_{\rm H\alpha,int}$ in the units of Watts) for the whole galaxy using their *k*-corrected absolute magnitudes (M_r), and emission-line EWs. A correction for the missing flux due to aperture effects is applied to each galaxy, using M_r to estimate the continuum at the wavelength of Hα. This approach of applying aperture corrections to individual galaxies, described in detail in Hopkins et al. (2003), yields similar results to the more complex colour gradient-based method described in Brinchmann et al. (2004). This type of aperture correction can underestimate emission-line luminosity (Gerssen, Wilman & Christensen 2012); however, such effects are likely to be minimal in this analysis as we are using a large sample of galaxies. The relation from Hopkins et al. (2003) is

$$L_{\rm H\alpha,int} = ({\rm EW_{H\alpha}} + {\rm EW_c}) \times 10^{-0.4(M_r - 34.10)} \times \frac{3 \times 10^{18}}{[6564.61(1+z)]^2} \left(\frac{F_{\rm H\alpha}/F_{\rm H\beta}}{2.86} \right)^{2.36}. \quad (1)$$

A constant correction for stellar absorption ($\rm EW_c = 2.5$ Å) in Balmer emission-line EWs is assumed for the calculation of luminosities for the GAMA galaxies (Hopkins et al. 2013). This value is chosen by comparing a sample of line fluxes used in this study against a robust sub-sample of line measurements using GANDALF (Sarzi et al. 2006). The choice of the stellar absorption correction, however, does not significantly affect the resulting LFs as shown in Fig. A1.

Stellar absorption-corrected emission-line fluxes are used in the determination of Balmer decrements (ratio of Hα to Hβ fluxes, $F_{\rm H\alpha}/F_{\rm H\beta}$) for each object in the two galaxy samples,

$$\frac{F_{\rm H\alpha}}{F_{\rm H\beta}} = \frac{\frac{({\rm H\alpha EW + EW_c})}{\rm H\alpha EW}}{\frac{({\rm H\beta EW + EW_c})}{\rm H\beta EW}} \times \frac{f_{\rm H\alpha}}{f_{\rm H\beta}}, \quad (2)$$

where, $f_{\rm H\alpha}$ and $f_{\rm H\beta}$ denote the measured emission-line fluxes. The dust obscuration in the Balmer lines Hα and Hβ can be determined from the comparison of measured Balmer decrements (BDs) with the Case B recombination theoretical value of 2.86 at an electron temperature of 10^4 K and an electron density of $100\,{\rm cm^{-2}}$ (Osterbrock 1989). The departure of the BD from 2.86 can be used to correct for the dust extinction intrinsic to the galaxy. The exponent of the BD in equation (1) is defined to be $k(\lambda_{\rm H\alpha})/[k(\lambda_{\rm H\beta}) - k(\lambda_{\rm H\alpha})]$, where $k(\lambda)$ is determined from the Cardelli, Clayton & Mathis (1989) Galactic dust extinction curve.

A small subset of galaxies in the GAMA and SDSS samples (13 and 4 per cent, respectively) have BDs < 2.86. BDs less than the theoretical Case B value can result from an intrinsically low reddening combined with uncertainty in stellar absorption, and also from errors in the line flux calibrations, and measurements (Kewley et al. 2006). Although, some of these low values are probably a result of galaxies hosting H II regions with high electron temperature, for which the theoretical Hα/Hβ ratio is lower than 2.86 (López-Sánchez & Esteban 2009). These galaxies are included in the final GAMA and SDSS samples, assuming no obscuration (i.e. BD is set to 2.86).

The SFRs in units of $\rm M_\odot\ yr^{-1}$ are derived using the calibration (Wijesinghe et al. 2011),

$${\rm SFR} = \frac{L_{\rm H\alpha,int}}{3.43 \times 10^{34}\,{\rm W}}, \quad (3)$$

which assumes the IMF definition of Baldry & Glazebrook (2003).

The majority of the SFR measurements reported in the literature use the Kennicutt (1998) calibration based on the Salpeter (1955) IMF. The SFRDs reported in this paper assume a slightly flatter than Salpeter IMF, taken from Baldry & Glazebrook (2003). The motivation here is the observed GAMA SFR–IMF relationship (Gunawardhana et al. 2011), where moderate-to-high SFR galaxies are characterized with flatter than Salpeter IMFs. The ratio of the calibration given in equation (3) to the Kennicutt (1998) calibration is $\sim$2.4 with our derived SFRs being lower than if the Kennicutt (1998) calibration had been used. We use the SFR calibration based on the Baldry & Glazebrook (2003) IMF throughout this paper,

[5] http://sdss.physics.nyu.edu/vagc/

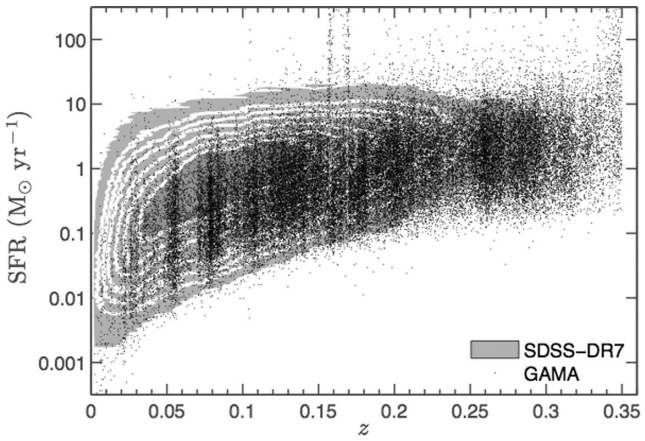

Figure 1. SFR versus redshift distributions of GAMA (black data points) and SDSS-DR7 (grey contours) surveys. While GAMA spectra are telluric absorption corrected, given the deep magnitude limits of the survey many of our sources are at or close to the S/N limit. The applied telluric absorption correction can therefore be unreliable over the wavelength ranges of strong atmospheric absorption bands as can be seen by the slight drop in GAMA SFRs centred at $z \sim 0.16$, corresponding to the z range where redshifted Hα emission line overlaps with the O_2 atmospheric (A) absorption band. These galaxies are removed from our sample. The drop in SFRs evident at $z \sim 0.14$ is due to atmospheric absorption effects on Hβ. For these galaxies, we estimate BDs empirically, see Section 3.2. The SDSS sample is not limited by these constraints as the majority are bright sources with comparatively higher S/N than GAMA.

unless otherwise stated. The distributions of SFRs of the GAMA and SDSS samples are shown in Fig. 1.

3.2 Estimating BDs

The large number of weak emission-line galaxies observed in GAMA gives the opportunity to investigate nearby low-SFR systems (Brough et al. 2011), and the low-z evolution of the SFRD. As Hβ is a considerably weaker emission feature than Hα, not all weak Hα sources in our final GAMA/SDSS samples have measured Hβ fluxes (Table 1). The distributions of GAMA star-forming galaxies with and without measured BDs in several redshift bins are shown in Fig. 2, and detailed in Table 1. As expected the distributions of galaxies without BDs are skewed towards low-luminosity (weak line) galaxies in all redshift ranges.

For these galaxies, we estimate BDs using the observed relationship between BD and aperture-corrected luminosity (Fig. 3). The solid line in Fig. 3 indicates the least absolute deviation fit to the data:

$$\mathrm{BD}_{\mathrm{gama}} = \begin{cases} 1.003 \times \log L - 30.0 & \log L \geqslant 32.77, \\ 2.86 & \log L < 32.77. \end{cases} \quad (4)$$

A similar relationship is derived for the SDSS-DR7 sample using their BDs and aperture-corrected luminosities.

$$\mathrm{BD}_{\mathrm{sdss}} = \begin{cases} 0.761 \times \log L - 21.7 & \log L \geqslant 32.27, \\ 2.86 & \log L < 32.27. \end{cases} \quad (5)$$

This relationship is then used to estimate BDs for the SDSS galaxies without BDs.

As the GAMA and SDSS surveys probe different star-forming populations, we do not attempt to determine a single fit to the data by combining GAMA and SDSS-DR7 data sets. In contrast to SDSS, the GAMA sample consists of more dust-obscured optically faint

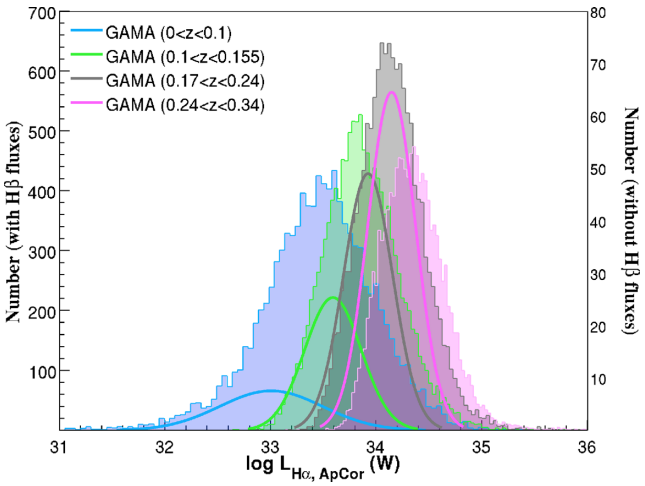

Figure 2. The distributions of aperture-corrected luminosities of galaxies with (histograms, with respect to the left y-axis scaling) and without (solid lines, with respect to the right y-axis scaling) measured BDs. For the galaxies without measured BDs, BDs are estimated using equation (4).

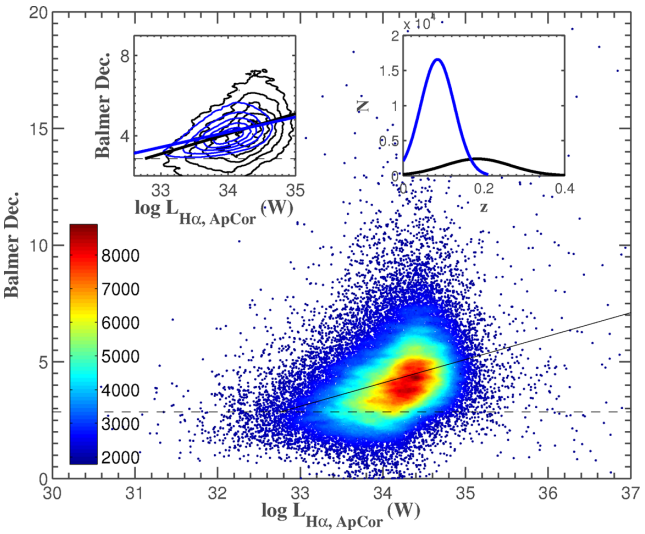

Figure 3. BD versus aperture corrected luminosity for the GAMA galaxies with measured BDs. The dashed line indicates the case B recombination value of 2.86, and the solid line shows the best-fitting linear relation to the data (equation 4). The color bar indicates the data density in units of per log $L_{\mathrm{H}\alpha,\mathrm{ApCor}}$ per BD. The two insets compare GAMA (black) and SDSS-DR7 (blue) samples. The left inset shows the BD versus aperture-corrected luminosity for GAMA and SDSS-DR7 star-forming samples, and their respective best-fitting linear relations. The difference between the two best-fitting relations is an indirect consequence of the different redshift distributions of the surveys, as shown in the right inset, leading to a sampling in GAMA of both higher SFR (more obscured) systems at higher redshift, as well as fainter (more obscured) systems at lower redshift.

galaxies at higher redshift, a single fit would, therefore, underestimate the empirical BD correction needed for GAMA galaxies as the fit would be heavily weighted by the relatively numerous SDSS galaxies.

Furthermore, we empirically estimate BDs for all the sources with measured BDs > 10 to avoid the sample being contaminated by sources with overestimated BDs, a result of weak Hβ measurements.

BD, as an indicator of dust obscuration, scales with both the SFR and redshift. High-SFR galaxies typically have greater obscuration than low-SFR systems (Hopkins et al. 2001; Afonso et al. 2003), and are generally found at higher redshifts. The insets in Fig. 3 illustrate this point. GAMA galaxies with higher $\langle z \rangle \approx 0.2$ (and therefore higher average SFRs) than SDSS ($\langle z \rangle \approx 0.08$) have relatively high BD values.

While only a small percentage of objects are without BDs in GAMA/SDSS samples, this small percentage consists mostly of low-z, low-luminosity systems. We demonstrate, in Section A2 below, that the impact of empirically assigning BDs on our derived LFs is minimal.

4 THE LUMINOSITY FUNCTION

For the LF estimates, we use the $V_{\rm max}$ (Schmidt 1968) method. In this section, we describe the derivation of $V_{\rm max}$ for galaxies in our sample subject to our selection criteria. We then detail the estimation of the LFs.

4.1 Derivation of volume corrections

The Hα LF, $\Phi(L)$, is defined as the number of star-forming galaxies per unit volume per unit luminosity (Schmidt 1968), and has the general form,

$$\Phi[\log L(H\alpha)] \times \Delta L = \frac{4\pi}{\Omega} \sum_i \frac{1}{V_{i,\rm max}}. \quad (6)$$

In this equation, $V_{i,\rm max}$ represents the maximum volume out to which the ith object would be visible to and still be part of the survey, ΔL and Ω define the assumed luminosity bin width and surveyed solid angle, respectively.

The Hα star-forming samples used in this study are subject to several selection constraints. For the GAMA sample, these are the two different r-band magnitude limits ($r < 19.4$ for G09, 15 and $r < 19.8$ for G12) of the survey (Driver et al. 2011), and the emission-line selection. Similarly for the SDSS-DR7, the emission-line selection and $r < 17.77$ magnitude limit. Given these constraints, the definition of $V_{i,\rm max}$ is

$$V_{i,\rm max} = \min[(V_{i,\rm max,H\alpha}), (V_{i,\rm max,}{}_r), (V_{i,z_{\rm lim}})] \times c_i, \quad (7)$$

where $V_{i,\rm max}$ is the minimum of the maximum volumes that the ith galaxy would have given the flux limit ($V_{i,\rm max,H\alpha}$), and magnitude limit ($V_{i,\rm max,}{}_r$) of the surveys, and c_i denotes the completeness correction.

The completeness corrections are made to each galaxy by weighting object numbers by the known missing fraction brighter than the survey magnitude. As noted in Jones & Bland-Hawthorn (2001), this type of a correction accounts for the survey incompleteness relatively accurately provided the observed fraction of galaxies is large. This is certainly the case with GAMA, which has a spectroscopic completeness >98 per cent (Driver et al. 2011).

The three main sources of incompleteness, as identified by Loveday et al. (2012) for the GAMA sample, are imaging incompleteness, spectroscopic incompleteness and redshift success. A correction for the imaging incompleteness (C_{im}) is estimated from fig. 1 of Loveday et al. (2012), while an empirical correction for both spectroscopic incompleteness and redshift success ($C_{\rm spec,}{}_z$) is applied based on the detection probability of a galaxy in the r-band Petrosian magnitude and $g - r$ colour in a given GAMA field. This correction is estimated relative to the GAMA tiling catalogue (Robotham et al. 2010; Loveday et al. 2012) and accounts for the missing sets of data (i.e. 2dFGRS, MGC), see Figs 4(a) and 5. The final weighting is given as

$$W = \frac{1}{C_{im}\, C_{\rm spec,}{}_z}. \quad (8)$$

A similar completeness correction for the SDSS-DR7 is also implemented. $C_{\rm spec,}{}_z$ correction is based on the SDSS-DR7 main galaxy spectroscopic sample chosen from the photometric catalogues. Similarly to GAMA, $C_{\rm spec,}{}_z$ correction for SDSS-DR7 takes into account 2dFGRS, PSCz and RC3 sources that are not part of our sample, see Fig. 4(b). The imaging incompleteness correction (C_{im}) for SDSS-DR7 is derived from Blanton et al. (2005).

4.1.1 *Broad-band volume corrections*

The determination of $V_{i,\rm max,}{}_r$ for the SDSS sample is relatively straightforward given the single magnitude limit of the survey. For GAMA galaxies, however, we estimate $z_{\rm max}$, at which that galaxy would still satisfy the $r < 19.4$ (for G09 and G15 fields) or $r < 19.8$ (for G12) selection criteria. The $z_{\rm max}$ values have been derived using the stellar template spectrum that best fits u,g,r,i,z photometry (StellarMassesv08; Taylor et al. 2011). Note that the values of $z_{\rm max}$ are flow corrected (Baldry et al. 2012). $V_{i,\rm max,}{}_r$ for GAMA becomes

$$V_{i,\rm max,}{}_r = \frac{2}{3}(V_{i,\rm max,}{}_{r=19.4}) + \frac{1}{3}(V_{i,\rm max,}{}_{r=19.8}). \quad (9)$$

A similar functional form to this is used in the derivation of $V_{i,\rm max,H\alpha}$.

4.1.2 *Emission-line volume corrections*

Due to the magnitude-limited nature of the GAMA/SDSS surveys, an approximate Hα flux limit of $F(\rm H\alpha) = 1 \times 10^{-18}$ W m^{-2} uncorrected for dust obscuration is assumed for the calculation of $V_{i,\rm max,H\alpha}$ (see Brough et al. 2011). This value roughly corresponds to the turn-over in the observed Hα flux histogram, and we assume that our sample is incomplete below this limit. Fig. 6 illustrates the distribution of SFRs in redshift relative to the SFR corresponding to the assumed flux limit. The impact of our assumptions about the Hα flux limit is minimal. This is detailed in Section 4.4.1.

4.2 Hα LFs

Hα LFs in several redshift bins are generated using the $V_{\rm max}$ technique described above and are shown in Fig. 7. The uncertainties in each luminosity bin are Poisson errors. The four panels in Fig. 7 show GAMA LFs in four redshift bins (blue points: $0 < z < 0.1$, $0.1 < z < 0.15$, $0.17 < z < 0.24$ and $0.24 < z < 0.35$), and SDSS LFs in two redshift bins (orange points: $0 < z < 0.1$ and $0.1 < z < 0.2$). The break in redshift between second and third GAMA redshift bins corresponds to the $z \sim 0.16$ region where Hα measurements are likely to be affected by the atmospheric O_2 absorption, see Fig. 1.

All GAMA LFs extend approximately an order of magnitude brighter in luminosity than other published LFs shown in Fig. 7. The GAMA low-z LF (Fig. 7a) extends approximately an order of magnitude in luminosity both fainter and brighter than other published results to date. Furthermore, our result agrees well with other studies in the luminosity range probed by existing data, with

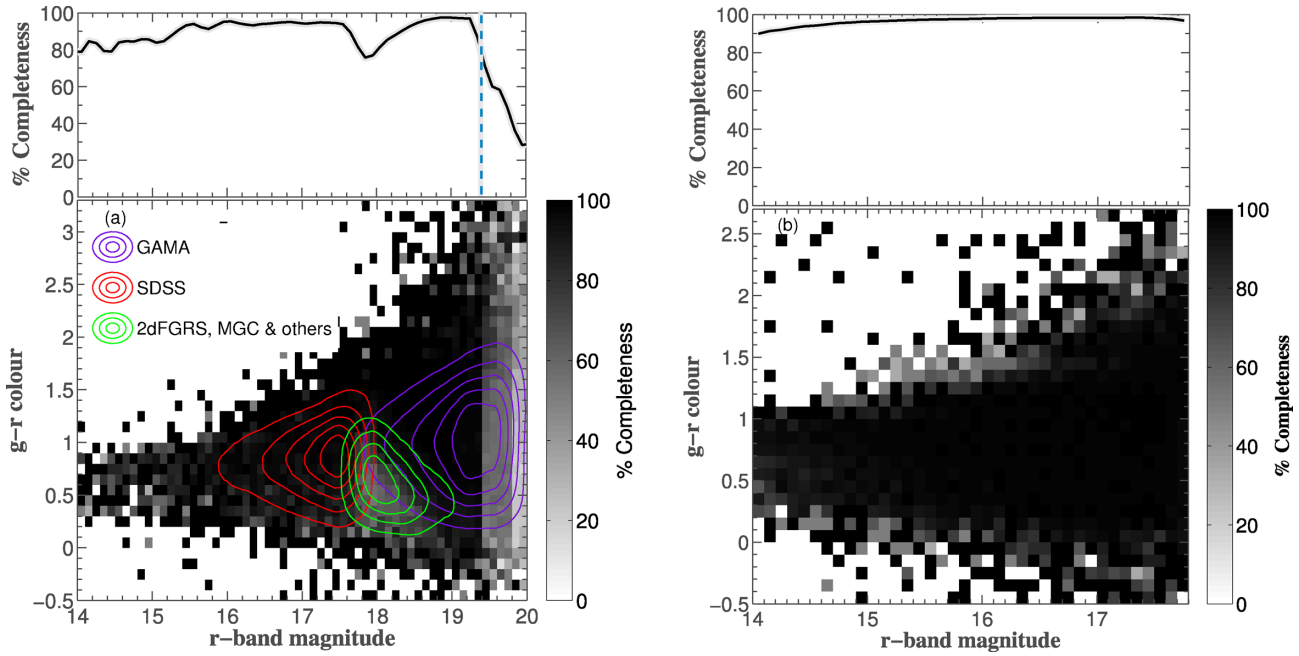

Figure 4. A correction ($C_{\mathrm{spec},z}$) based on the distribution of galaxies in r-band Petrosian magnitude and $g-r$ colour is applied to the LFs to account for the spectroscopic incompleteness and redshift success rate. This correction also takes into account the sample incompleteness due to the lack of 2dFGRS, MGC and 6-degree Field Galaxy Redshift Survey (6dFGRS) data. The panels (a) and (b) indicate the percentage completeness (grey-scale) at a given r-band magnitude and $g-r$ colour bins for the complete GAMA and SDSS-DR7 samples, respectively. Bin widths in r-band magnitude and $g-r$ colour are 0.1. The purple and red contours shown in (a) indicate the distributions of objects observed by GAMA and SDSS surveys, and the green contours correspond to the spectra we were not able to measure flux-calibrated lumnosities, and are not included in our sample. $C_{\mathrm{spec},z}$ as a function of r-band magnitude is shown in the top panel.

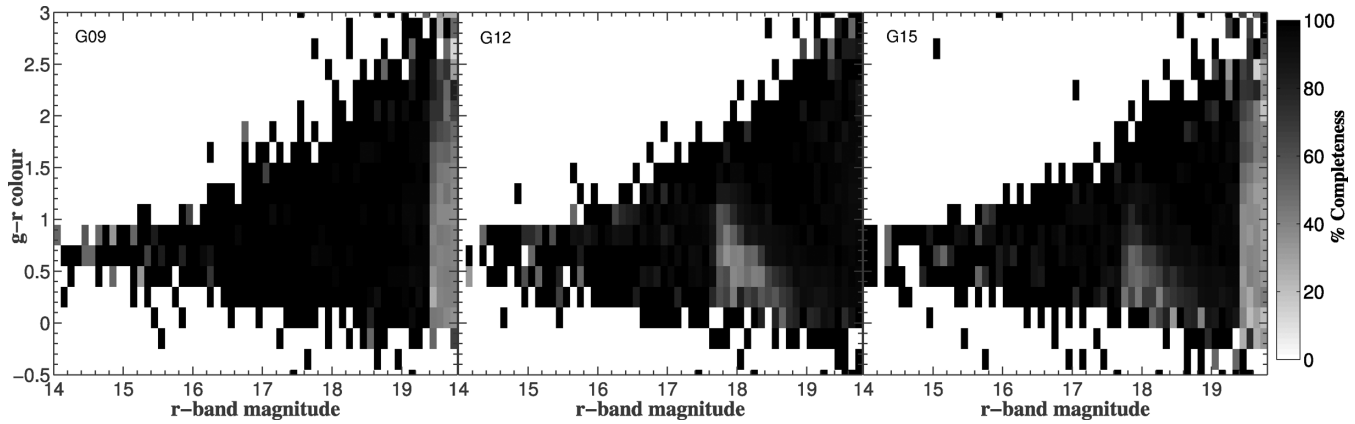

Figure 5. $C_{\mathrm{spec},z}$ corrections for each of the GAMA fields separately. The 2dFGRS and MGC survey areas do not overlap with the GAMA-09 hr region. The incompleteness around $(r, g-r) \sim (18, 0.5)$ in GAMA-12 hr and -15 hr regions is due to the lack of Hα measurements from the 2dFGRS and MGC surveys.

the exception of the Westra et al. (2010) LF. The disagreement between the GAMA and Westra et al. (2010) LFs is largest over the shaded region. This could be due to the relatively small survey area ($\sim$4 deg^2) of Westra et al. (2010) sampling an underdense region. We demonstrate in Section 4.3, however, that there may be a significant impact from the joint r band and emission-line selection, and the assumptions related to Hα flux limits for magnitude-limited surveys that contribute to this disagreement. These are likely to be the dominant effects.

The SDSS-DR7 LF explores a similar range in bright luminosities as GAMA and agrees well with both GAMA and published LFs. The turn-over below $L_{\mathrm{H}\alpha} \approx 10^{31.5}$ W in the SDSS LF is due to the incompleteness arising from the Hα line flux limit.

The GAMA LF over $0.1 < z < 0.15$ (Fig. 7b) is in good agreement with the SDSS-Stripe 82 $0.032 < z < 0.2$ LF of Gilbank et al. (2010) within $33 \leq \log L_{\mathrm{H}\alpha} \leq 35.5$. The disagreement between the GAMA and SDSS LFs in the second redshift bin is likely due to the brighter SDSS magnitude cut ($r = 17.77$) preventing optically faint high-SFR galaxies from entering the SDSS sample (see discussion in Section 4.3). This assertion is supported by the lack of evolution between $0 < z < 0.1$ and $0.1 < z < 0.2$ SDSS LFs. The scatter in published LFs is significant over $0.1 < z < 0.3$, particularly at relatively low luminosities, where cosmic (sample) variance, selection and incompleteness issues impact the most. The GAMA LF in the $0.17 < z < 0.25$ redshift bin certainly provides a better estimate for the bright end of the LF, where other LFs suffer from small

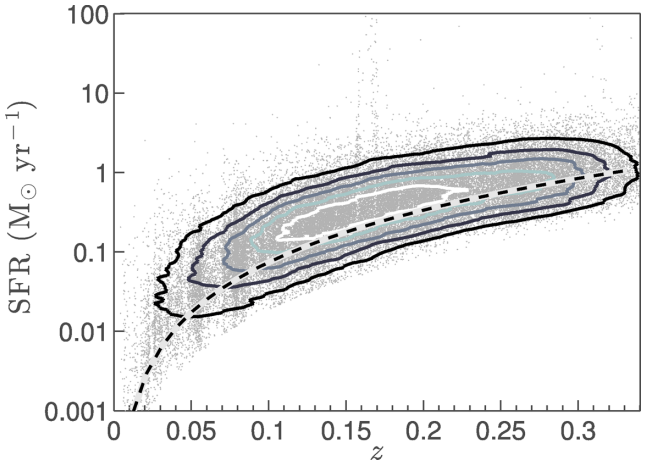

Figure 6. The distribution of the observed (i.e. not corrected for dust obscuration) Hα SFRs (data points and the contours) relative to the SFR corresponding to the assumed flux limit of 1×10^{-18} W m^{-2} (dashed line). Close to half of the sources with detected Hα emission lie below the selected Hα completeness limit. Note that all the SFR points shown in Fig. 1 are also shown here. See Fig. 1 caption for more information.

number statistics. The final GAMA LF agrees well with Westra et al. (2010) at this redshift. This agreement, however, is likely to be a consequence of the bivariate selection of the GAMA sample, as discussed in the next section. The agreement is therefore likely an outcome of both surveys preferentially selecting brighter galaxies at higher redshifts.

4.3 Bivariate selection

Both GAMA and SDSS are magnitude-limited surveys and any emission-line sample drawn from such a survey is subject to dual selection criteria. In order to contribute to the LF, a galaxy must satisfy both the broad-band magnitude limit and the emission-line flux limit. The completeness corrections applied to the Hα LFs account for the incompleteness as a function of broad-band magnitude and colour, but nonetheless a bias remains. There is a population of bright Hα galaxies that do not enter the sample initially as their broad-band magnitudes are too faint, and it is not possible to correct for this effect. We explore the impact of this bias here.

We assume a fiducial Hα flux limit of 1×10^{-18} W m^{-2} for the analysis presented in this paper (Brough et al. 2011), which also approximately corresponds to the turn-over in the observed flux histogram, see Fig. 10. As discussed above in Section 4.4.1, the incompleteness increases towards the flux limit, and can be as large as 50 per cent at the limit. The effect of Hα incompleteness becomes progressively larger with redshift. As such, the GAMA and SDSS-DR7 low-redshift samples are likely to be the most complete, with the higher redshift GAMA and SDSS samples becoming more and more incomplete with increasing redshift.

In Fig. 8, we show the bivariate Hα/M_r distributions for our GAMA and SDSS samples. These are not bivariate LFs, which we present in a companion paper (Gunawardhana et al., in preparation), but serve to show the distribution of luminosities spanned by the galaxies detected in each sample.

Fig. 8(a) shows the bivariate Hα luminosity/M_r distribution for both the GAMA and SDSS $z \leq 0.1$ samples. The overlapping region of the bivariate distributions indicates that the GAMA sample consists of optically faint galaxies with similar SFRs to optically bright SDSS galaxies. This r-band faint population is only detected in GAMA, demonstrating the Hα incompleteness of SDSS. The grey band in Fig. 8(a) highlights the same luminosity range emphasized by the shaded region in Fig. 7(a), where the discrepancy between the Westra et al. (2010) and GAMA/SDSS-DR7 LFs is greatest.

The effects of joint selection on the higher redshift LFs are evident in Figs 8(b) and 9. Only the distribution of the low-z sample covers a wide range in both Hα luminosity and M_r, while the higher redshift distributions become progressively more and more limited in the range of both Hα luminosity and M_r probed; each sample is missing a fraction of highly star forming, but optically faint galaxies, and this missing fraction becomes more significant with increasing redshift. The impact, then, is that our higher redshift LFs remain incomplete, and can potentially be missing as much as 50 per cent of the bright Hα population. This is explored in more detail in Gunawardhana et al. (in preparation), which investigates the evolution of the bivariate Hα/M_r LF.

4.4 Lower and upper limits of Hα LFs

In addition to the incompleteness introduced by the bivariate selection, where optically faint star-forming galaxies do not enter our sample due to the broad-band selection of the survey, further uncertainties arise from the adopted $V_{\rm max}$ definition. Here, we investigate a series of $V_{\rm max}$ corrections to the LFs that bracket our best estimated LFs presented in Section 4.2. The aim of this analysis is to identify the (extreme) lower and upper limits to SFRDs. In subsequent sections, we show that the uncertainties related to measurements and systematics fall within these limits.

4.4.1 Best estimate

First, we present a discussion of the true LFs presented in Section 4.2 that assume a flux limit of 1×10^{-18} W m^{-2}, and explain the discrepancies between GAMA and Westra et al. (2010) $0 < z < 0.1$ LFs shown in Fig. 7.

Emission-line samples drawn from magnitude-limited surveys, such as GAMA and SDSS, involve assumptions about flux limits. The point at which an observed flux histogram turns over can be taken as a suitable limit. We assume an Hα flux limit of 1×10^{-18} W m^{-2} (Brough et al. 2011) to produce the results presented in Section 4.2 following the methodology described in Section 4.1. This limit roughly corresponds to the peak value of the observed low-z Hα flux histogram (Fig. 10a).

The open histogram in Fig. 10 depicts the predicted distribution of Hα fluxes over the same redshift range. This distribution is a simple prediction based on the GAMA low-z Hα LF presented in Section 4.2. This prediction of the flux distribution is derived from the LF that we calculate from the observed flux distribution, and is thus being used merely as a self-consistency test. In the absence of the true underlying flux distribution, this is sufficient, though, to explore our expected completeness as a function of Hα flux, and we can see that even at the peak of the observed flux distribution, we are only about 75 per cent complete. At our assumed flux limit of 1×10^{-18} W m^{-2} we are about 50 per cent complete. To investigate how our assumptions about the Hα flux limit influence the shape of the LF, we reproduce the low-z GAMA Hα LF assuming several different flux limits indicated in Fig. 10(a). The resultant LFs are shown in Fig. 10(b), and it can be seen that the changes are primarily at the fainter end of the LF (log $L \lesssim 34$).

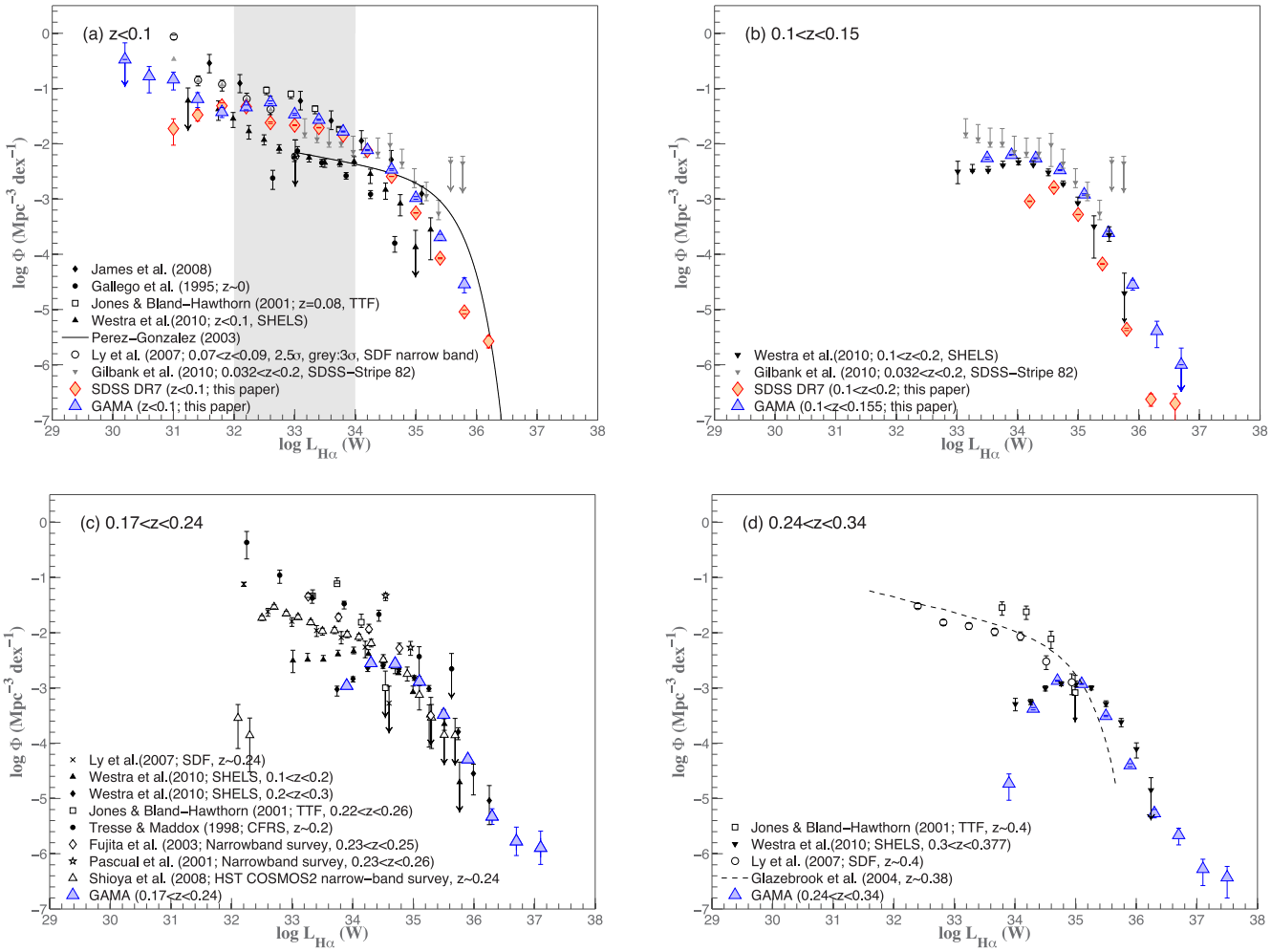

Figure 7. GAMA (blue) and SDSS-DR7 (red) Hα LFs in four broad redshift bins (see key in each panel for detailed ranges). The redshift ranges increase from left-to-right, top-to-bottom, covering a total redshift range of $0 < z < 0.34$ for GAMA and $0 < z < 0.2$ for SDSS-DR7. The axis ranges in each panel are kept the same to highlight the broad luminosity range sampled by the GAMA LFs. The figure also presents a comparison of our results with published LFs spanning similar redshift ranges. LFs from other authors have been converted to our assumed cosmology. An obscuration correction based on the assumption of a one magnitude extinction in Hα (Hopkins & Beacom 2006) is applied to correct the observed LFs of Jones & Bland-Hawthorn (2001) and Gilbank et al. (2010). The grey band in (a) highlights the luminosity range over which the discrepancy between Westra et al. (2010) and GAMA low-z LFs is largest.

We assert that the differences in the assumed Hα flux limit and in the formulation of V_{max} between this analysis and Westra et al. (2010) contribute to some of the discrepancies between LFs shown in Fig. 7(a). Westra et al. (2010) have used a lower Hα flux limit to construct their LFs. A low-flux limit yield a larger volume over which an object could be detected, resulting in a lower LF normalization. We demonstrate this in Fig. 10(b) by varying the flux limit. Note that in this study, a flux limit lower than 1×10^{-18} W m^{-2} yield a V_{max} limited by r band (see equation 7). These differences in methods along with the uncertainties arising from the cosmic (sample) variance could explain the discrepancy between GAMA low-z and Westra et al. (2010) LFs (Fig. 7a).

4.4.2 Identifying a lower limit

In order to identify a lower limit to SFRD, we set the Hα flux limit to be equal to our Hα detection limit of 2.5×10^{-19} W m^{-2}. This is an unrealistically low limit as the observed Hα flux histogram in comparison to that predicted indicates close to 90 per cent incompleteness in Hα detections (Fig. 10a). Additionally, we apply no r-band V_{max} constraint or completeness corrections to the LFs.

Intentionally, neglecting the r-band volume limits and completeness correction ensure that the resulting LF will underestimate the true values, and should be a strong lower limit (Fig. 10b). The integral of this resulting LF in turn will give a strong lower limit to the SFRD. The Hα LFs constructed this way are shown in Figs 10(b) and 11. The lower limit number densities indicated by data points in Fig. 11 are generally lower than that predicted by the best estimate LFs at a given luminosity. This is, however, not always true as can be seen in Fig. 11(d) where the red points at $\log L \approx 34$ (W) and $\log L > 37$ (W) indicate higher number densities than the best estimate LF points. As a result of the low-flux limit, a large number of low-Hα flux detections enter the sample. Most of these objects are low-luminosity galaxies such that the number of galaxies contributing to the lower limit LF point at $\log L \approx 34$ (W) is relatively larger than the number contributing to the best estimate LF data point. The total number of galaxies contributing to the best

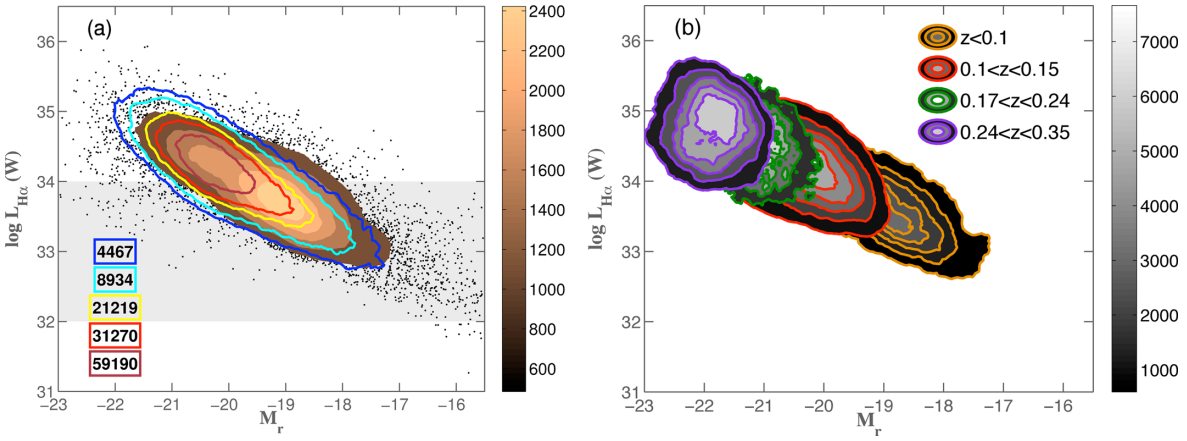

Figure 8. GAMA absolute magnitude (M_r) versus aperture- and obscuration-corrected Hα luminosity ($L_{\mathrm{H}\alpha}$) bivariate distributions. (a) The distribution of GAMA galaxies within $0 < z < 0.1$ with $r < 19.4$ (or 19.8), compared with SDSS galaxies in the same redshift range with $14.5 < r < 17.77$. The grey band highlights the same luminosity range as in Fig. 7(a). The GAMA distribution is represented by solid contours and data points, while the SDSS distribution is represented by transparent coloured contours. The brown colour bar indicates the data density colour coding for the GAMA contours, while the data densities corresponding to the SDSS contours are shown in the key. The unit of data density is per M_r per log $L_{\mathrm{H}\alpha}$. (b) The Hα luminosity versus M_r distributions for the GAMA sample in the four redshift ranges.

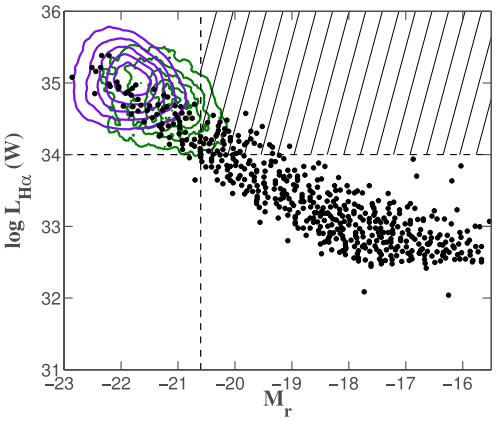

Figure 9. GAMA absolute magnitude (M_r) versus aperture- and obscuration-corrected Hα luminosity ($L_{\mathrm{H}\alpha}$) bivariate distributions for galaxies in $0.17 < z < 0.24$ (green) and $0.24 < z < 0.34$ (purple) redshift bins compared to the distribution presented in fig. 9 of Shioya et al. (2008). They used *HST* COSMOS2 narrow-band survey data to construct their Hα LF. The redshift coverage of their data is ∼0.24. The vertical dashed line indicates the approximate absolute r-band magnitude corresponding to $z \sim 0.24$ given GAMA's limiting magnitude of 19.8. The horizontal line marks the approximate luminosity around the 'knee' (i.e. close to L^*) of higher z LFs. This figure demonstrates that there is a population of optically faint star-forming galaxies with $z \sim 0.24$ (close to 50 per cent) that do not enter either $0.17 < z < 0.24$ or $0.24 < z < 0.34$ GAMA samples.

estimate LF at $\log L > 37$ (W) are both lower and their $V_{\max}$ are closer to $V_{i,z\mathrm{lim}}$ (see equation 7), whereas the number contributing to the lower limit LF at $\log L > 37$ (W) is slightly larger with $V_{\max}$ approximately equal to $V_{i,z\mathrm{lim}}$.

4.4.3 Identifying an upper limit

An upper limit to SFRD is determined by including all Hα detections down to our detection limit. The $V_{\mathrm{max,\,H}\alpha}$ for objects with fluxes between the assumed detection limit and flux limit are set to equal to their comoving volumes. The resultant LFs are shown in Figs 10(b) and 11. Note that this is not a substantial increase over our best estimate LF. The addition of all reliable Hα-detected sources, those below the nominal flux limit, does not significantly increase the LF or the corresponding SFRD.

5 FUNCTIONAL FITTING

Galaxy LFs are usually fitted with a Schechter (1976) function (e.g. Loveday et al. 1992; Blanton et al. 2003),

$$\Phi(L)\mathrm{d}L = \Phi^* \left(\frac{L}{L^*}\right)^{\alpha} \exp\left(-\frac{L}{L^*}\right) \mathrm{d}\left(\frac{L}{L^*}\right), \tag{10}$$

where L is the galaxy luminosity, and $\Phi(L)\,\mathrm{d}L$ is the number of galaxies in luminosity range $L + \mathrm{d}L$ per cubic Mpc. The parameters α, L^* and Φ^*, determined empirically, describe the shape of the fit, the slope of the LF at faint luminosities, the characteristic Schechter luminosity, and the normalization factor at L^* respectively.

The same functional form is generally used to fit star-forming LF data (e.g. Gallego et al. 1995; Jones & Bland-Hawthorn 2001). However, in contrast to broad-band optical LFs, our measured Hα LFs are inconsistent with an exponential drop in number density for $L > L^*$. Most of the published Hα LFs for star-forming galaxies only probe a limited range in luminosity centred around L^*. Within this narrow range probed, the Schechter function provides a good fit. The much larger volumes probed by the GAMA and SDSS–DR7 LFs allow us to sample a wide range in Hα luminosities. This enables us for the first time to study both faint and bright ends of the Hα LF. For these LFs, the Schechter function is clearly not the best representation. This can be best seen in Fig. 7(a) by comparing GAMA and SDSS LFs with the Pérez-González et al. (2003) LF, the exponential drop of the Schechter function is too steep to match the LFs presented in this paper.

We find that the functional form presented in Saunders et al. (1990) provides a more suitable fit to the GAMA LFs,

$$\Phi(L)\mathrm{d}L = C \left(\frac{L}{L^*}\right)^{\alpha} \exp\left[-\frac{1}{2\sigma^2}\log^2\left(1+\frac{L}{L^*}\right)\right] \mathrm{d}\left(\frac{L}{L^*}\right). \tag{11}$$

Motivated by the power-law shape of the far-infrared 60 μm LFs for $L > L^*$, Saunders et al. (1990) introduced the above function,

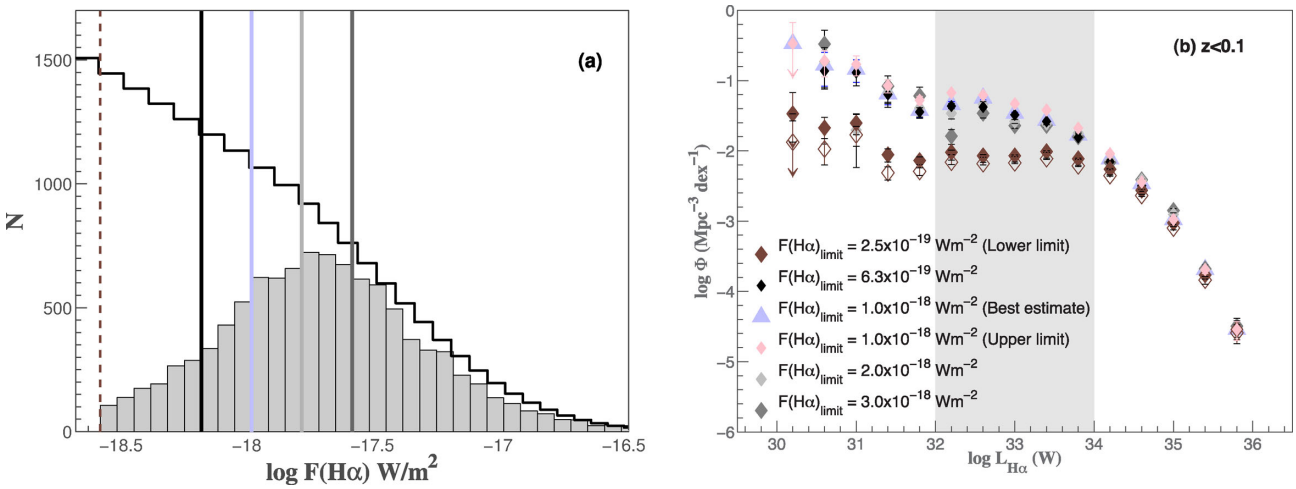

Figure 10. The observed versus predicted flux Hα flux distributions for low-redshift galaxies. The solid histogram shows the observed Hα flux histogram for galaxies with $z < 0.1$. A simple prediction of the distribution of Hα fluxes for low-z galaxies based on our low-z Hα LF is shown by the open histogram. The blue vertical solid line indicates the Hα flux limit used in this study, and on the right the resultant low-z LF. The rest of the solid lines indicate different flux limits tested, and on the right the resultant LFs. The low-z LFs corresponding to the two limiting cases are shown here with (filled symbols) and without (open symbols) completeness corrections. The grey band highlights the same luminosity range as in Fig. 7(a).

which behaves as a power law for $L < L^*$ and as a Gaussian in $\log L$ for $L > L^*$ with a Gaussian width given by σ, and a normalization factor at L^* given by C. The SFRD is estimated from numerically integrating the Saunders et al. (1990) function. This functional form is widely used to describe the LFs of far-infrared, and radio star-forming populations (e.g. Rowan-Robinson et al. 1993; Hopkins et al. 1998). Using mock galaxy samples drawn from a Shechter stellar mass distribution Salim & Lee (2012) demonstrate that the underlying SFR distribution is better described with a Saunders function while a Shechter function provides a good description for mass distributions. They have also shown that a star forming LF can appear Shechter-like when luminosities are not corrected for the dust obscuration.

In particular, it is encouraging that this functional form can be used consistently to reproduce the LFs for SFR tracers at each of the radio, far-infrared and now Hα wavelengths. We highlight here that while Schechter functions have been used in the past to fit the shape of the Hα LF, the surveys in question have all probed relatively small volumes compared to GAMA and SDSS. Only with a sufficiently large volume is the bright end of the star-forming population able to be sufficiently well sampled to reliably measure the rare extreme star-forming population. Even with a Saunders parametrization, it is still difficult to describe both the lowest SFR galaxies contributing to the faint-end rise in Φ and the highest SFR galaxies that diverge from a Gaussian decline in Φ. Therefore, in order to constrain the functional fits to the LFs, the outlying GAMA LF points, shown as open symbols in Fig. 11, are excluded from the fitting. The variation in Hα luminosity density with Hα luminosity as traced by the LFs and the Saunders functional fits to data is shown in Fig. 14. See Section A3 for comparisons with the Schechter functions. The fact that a Saunders functional form seems to be the most appropriate form for each of radio, far-infrared and Hα LFs suggests that the same should be true for ultraviolet LFs probing star formation in galaxies. This is again demonstrated in Salim & Lee (2012) using mock galaxy samples. They find that intrinsic ultraviolet LFs over a moderate dynamic range follow their mock SFR functions, and indicate a Saunders-like drop in number densities with increasing luminosities. This could have a potentially significant impact on the very highest redshift estimates of SFRD, where UV LFs are often fitted by Schechter functions (e.g. Bouwens et al. 2010, 2011) to data measured over a comparatively narrow range of observed luminosity.

5.1 Fits to the data

We use a Levenberg–Marquardt method for finding the minimum χ^2 fit to the binned LF data points. The resultant Saunders functional fits and the best-fitting parameters to the GAMA/SDSS LFs are presented in Fig. 11 and Table 2.

All GAMA LF data points and most of the SDSS LF data points belonging to the lowest-z bins are used in the fitting, see Fig. 11. None of the rest of our LFs cover the same wide range in luminosity that the GAMA low-z LF covers, largely due to the r-band flux limit in the survey selection (Fig. 9). As a consequence, we can only constrain the LF over a narrow range in luminosity at the higher redshifts. For instance, the range in luminosity sampled by the second GAMA LF is less than half the range sampled by the GAMA low-z LF (see Fig. 7). The lack of $L < L^*$ LF data is a significant drawback in determining α accurately. To overcome this difficulty, we investigated two alternative approaches to fitting the Saunders functional forms to LF data.

Fixed the faint-end slope of the LF. This is the approach shown in Fig. 12. We use the best-fitting α parameter from the Shioya et al. (2008) narrow-band LF ($z \sim 0.24$) to fix the faint-end of the higher-z GAMA/SDSS LFs. This value is chosen instead of that estimated using GAMA low-z LF or other narrow-band LFs estimates as the redshift range probed by the Shioya et al. (2008) LF roughly corresponds to the redshift range of the GAMA higher-z LF, and it probes a relatively larger luminosity range at that redshift. Narrow-band surveys, although only covering a comparatively small sky area, have the advantage of being complete down to a given Hα luminosity, and at modest redshifts, they successfully extend substantially below $L \ll L^*$ compared to those from surveys initially selected with a broad-band magnitude limit.

The LF data points that indicate a turn-over in number density as a result of higher-z sample incompleteness are excluded from the functional fits. These excluded points are denoted by open symbols in Fig. 11. Even though the faint-end slope of the LF is fixed, the

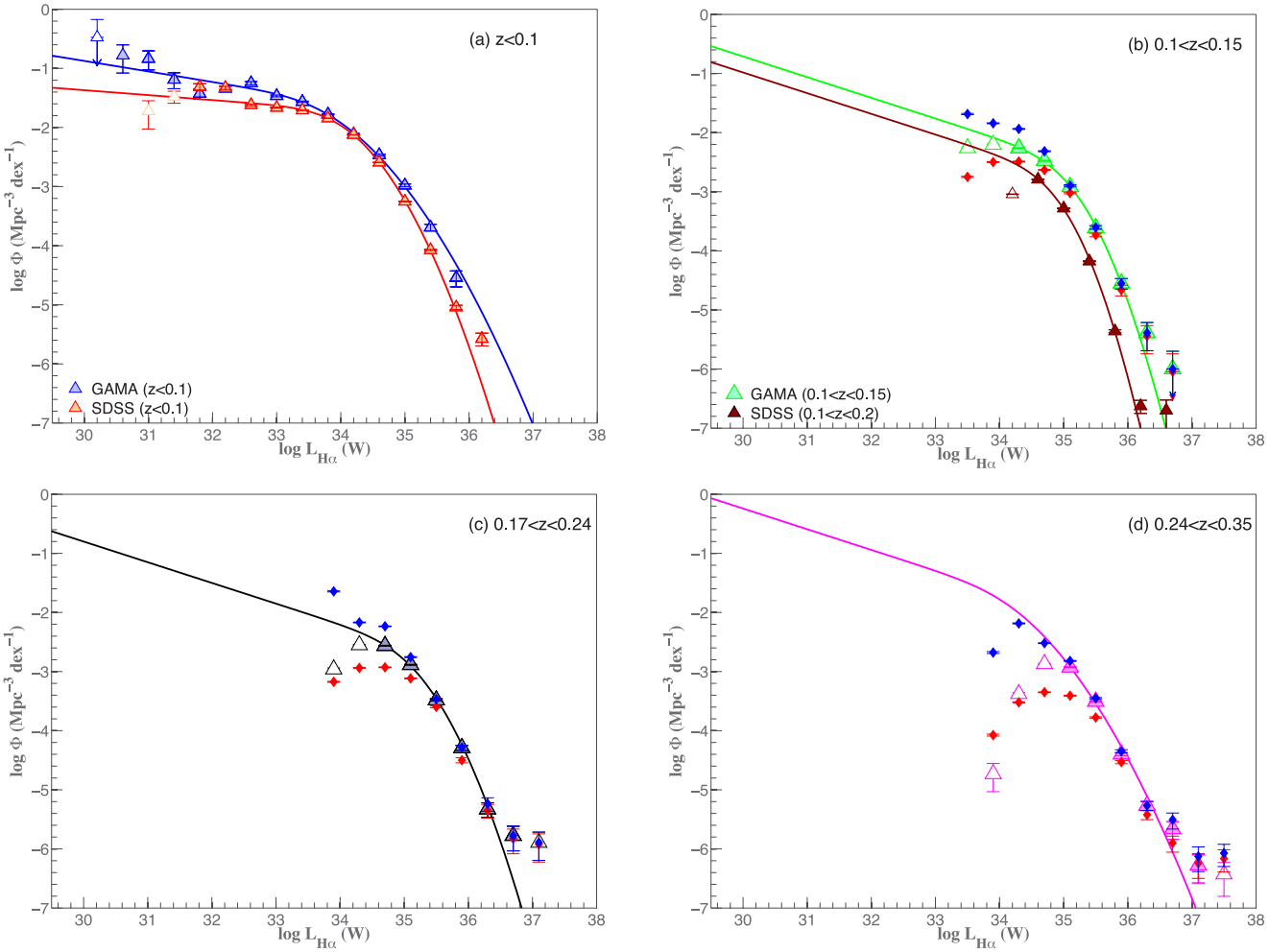

Figure 11. The best-fitting Saunders functions for all the LFs. The redshift increases from left-to-right, top-to-bottom. The triangles denote Φ values in each luminosity bin, with filled triangles showing the points used for the fit. The best-fitting α value from the Shioya et al. (2008) LF is used to constrain the faint-end slope of GAMA LFs beyond $z > 0.1$. The blue and red diamonds indicate the LFs corresponding to lower and upper limiting V_{max} cases discussed in Section 4.4, and the resulting SFRDs are shown in Fig. 15. The best-fitting Saunders parameters are given in Table 2.

Table 2. The best-fitting Saunders parameters for the LFs, corresponding SFRDs and their Poisson uncertainties.

z	log L* (W)	log C	α	σ	log SFRD (M$_\odot$ yr^{-1} Mpc^{-3})
$z < 0.1$ (GAMA, Fig. 11a)	33.00 ± 0.41	-1.77 ± 0.16	-1.16 ± 0.07	0.84 ± 0.09	-2.068 ± 0.010^a
$z < 0.1$ (SDSS-DR7, Fig. 11a)	33.43 ± 0.53	-2.02 ± 0.23	-1.08 ± 0.22	0.61 ± 0.08	-2.244 ± 0.010
$0.1 < z < 0.15$ (GAMA, Fig. 11b)	34.55 ± 0.85	-2.67 ± 0.83	-1.35^b	0.47 ± 0.18	-2.096 ± 0.004
$0.1 < z < 0.2$ (SDSS-DR7, Fig. 11b)^c	34.42 ± 1.46	-2.89 ± 1.99	-1.35^b	0.42 ± 0.25	-2.522 ± 0.002
$0.17 < z < 0.24$ (GAMA, Fig. 11c)	34.53 ± 0.74	-2.75 ± 0.73	-1.35^b	0.55 ± 0.17	-2.118 ± 0.004
$0.24 < z < 0.35$ (GAMA, Fig. 11d)^c	33.47 ± 3.56	-1.82 ± 4.14	-1.35^b	0.81 ± 0.52	-1.896 ± 0.004

^{a}An uncertainty of ∼15 per cent needs to be incorporated to this value to account for GAMA's known underdensity (Driver et al. 2011).
$^b\alpha$ is fixed to be −1.35 (Shioya et al. 2008).
^{c}The fit cannot be constrained as the LF turns-over at around L^*. This leads to very large uncertainties in the fitted parameters.

bright end of the LF is affected by the bivariate selection effects, which progressively become significant with redshift (Fig. 8b). This results in lower integrated SFRDs for the higher-z LFs as the bivariate selection prevents optically faint high-Hα luminosity objects from entering the higher-z samples, and affecting the overall normalization of the LF. The fitting for the highest-z LF cannot be constrained as only the points above the knee of the LF can be used.

Normalized to match narrow-band LF data.

Another way of determining the faint-end slope of the Hα LFs is to normalize our data to match narrow-band LFs. Narrow-band surveys are complete down to a given Hα luminosity and consist of relatively large number of faint Hα emitters (Fig. 9). As a result their LFs are more complete below $L < L^*$ than those based on a broad-band selected galaxy sample. In contrast, magnitude-limited surveys covering a large sky area consist of relatively large numbers of bright Hα sources, and the respective LFs are likely more complete above

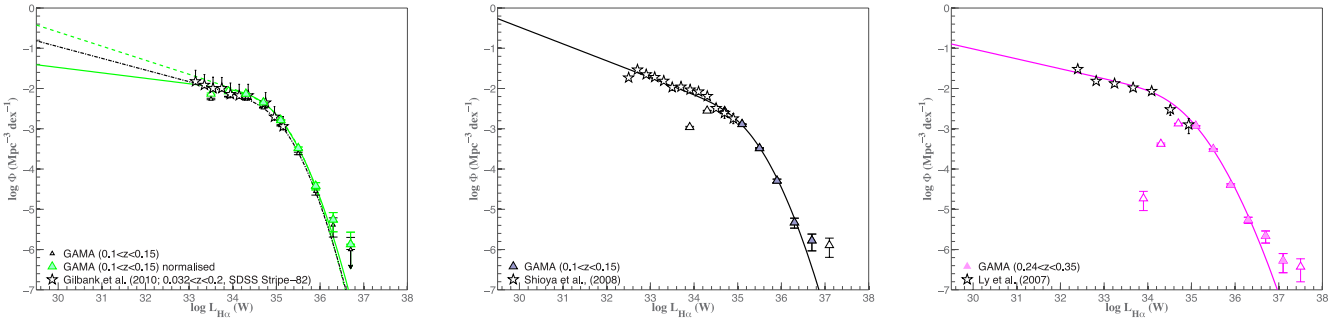

Figure 12. The best-fitting Saunders functions for the higher-z LFs. The triangles denote GAMA Φ values in each luminosity bin, with filled triangles showing the points used for the fit. We use the published LFs of Shioya et al. (2008, narrow-band survey, $0.233 < z < 0.249$), and Ly et al. (2007, narrow-band survey, $0.382 < z < 0.418$) to get a better estimate of the faint-end evolution of GAMA $0.17 < z < 0.24$ and $0.24 < z < 0.34$ LFs. For the GAMA $0.1 < z < 0.15$ LF, we have used the Gilbank et al. (2010, based on magnitude limited SDSS data, $0.032 < z < 0.2$) LF data as there are no wide-area narrow-band measurements are available. These points are shown as open stars in all panels. The normalization factor determined for $0.1 < z < 0.15$ range using Gilbank et al. (2010) is the largest (0.12 dex). This could be due to the differences in the redshift ranges probed the two LFs. The normalization determined for the $0.17 < z < 0.24$ range using Shioya et al. (2008) measurements is negligible, and a normalization cannot be determined for the final redshift bin as Ly et al. (2007) and GAMA $0.24 < z < 0.34$ LF data do not overlap. The colours correspond to those in Fig. 11. The best-fitting Saunders parameters are given in Table 3. For the GAMA $0.17 < z < 0.24$ combined LF, we provide the functional fits determined using *normalized* GAMA LF data combined with Gilbank et al. (2010) data and fixing the faint-end slope (α) at -1.35 (dashed line), fitting to the faint-end (solid line) and the original GAMA $0.1 < z < 0.15$ LF data combined with Gilbank et al. (2010) data and fitting to the faint-end slope (dot–dashed line).

Table 3. The best-fitting Saunders parameters and SFRDs for the combined LFs presented in Fig. 12.

z	log L^* (W)	log C	α	σ	log SFRD ($M_\odot$ yr^{-1} Mpc^{-3})
$0.1 < z < 0.15$ (dashed green line in Fig. 12)	34.62 ± 0.37	-2.58 ± 0.26	-1.35^a	0.45 ± 0.09	-1.973 ± 0.004
$0.1 < z < 0.15$ (solid green line in Fig. 12)	34.31 ± 0.61	-2.42 ± 0.35	-1.13 ± 0.38	0.51 ± 0.09	-1.996 ± 0.004
$0.1 < z < 0.15$ (dot–dashed black line in Fig. 12)	34.48 ± 0.63	-2.62 ± 0.48	-1.29 ± 0.36	0.48 ± 0.10	-2.105 ± 0.004
$0.17 < z < 0.24$	34.54 ± 0.32	-2.74 ± 0.24	-1.42 ± 0.08	0.57 ± 0.08	-2.077 ± 0.004
$0.24 < z < 0.35$	33.94 ± 0.88	-2.35 ± 0.53	-1.25 ± 0.34	0.68 ± 0.12	-2.056 ± 0.004

[a] α is fixed to be -1.35 (Shioya et al. 2008).

$L > L^*$ than those based on narrow-band data sets. We therefore use published narrow-band LF data to estimate the evolution of the faint-end of higher-z ($0.17 < z < 0.24$ and $0.24 < z < 0.34$) GAMA LFs. For the GAMA $0.1 < z < 0.15$ LF, where no wide-area narrow-band measurements are available, we combined GAMA LF data with Gilbank et al. (2010) data to determine the faint-end slope of the LF.

The overlapping LF data from Gilbank et al. (2010) and Shioya et al. (2008) are used to normalize the higher-z ($0.1 < z < 0.15$ and $0.17 < z < 0.24$) GAMA LFs. However, such a normalization could not be achieved for the highest-z ($0.24 < z < 0.34$) GAMA LF due to the lack of overlap between GAMA and Ly et al. (2007) LF. The normalization factors estimated using the approximately overlapping Gilbank et al. (2010) and GAMA $0.1 < z < 0.15$ LF data in $34 < \log L(W) < 35.5$ range (see Fig. 7b) is $\sim$0.12 dex, and the factor using overlapping Shioya et al. (2008) and GAMA $0.17 < z < 0.24$ LFs is negligibly small as the two LFs agree very well (Fig. 7c). We note that the larger normalization required to match GAMA $0.1 < z < 0.15$ LF data with Gilbank et al. (2010) LF could be a result of the different redshift ranges probed by the LFs. It is likely that Gilbank et al. (2010) LF indicates some evolution as it covers a larger redshift range than the respective GAMA LF. The functional fits to the combined LFs are shown in Fig. 12, and the best-fitting functional parameters are given in Table 3.

The modest level of evolution demonstrated by these LFs is highlighted in Fig. 13. The largest change is seen between the first and second redshift bins, with minimal measurable change thereafter. The lack of evolution here is most likely due to the high incompleteness of higher redshift samples, a result of the joint selection in both broad-band magnitude and emission-line flux. Even though there is some evolution in the LF over this redshift range, it is difficult to quantify the extent accurately without accounting for the impact of the sample selection. This has been outlined above in Section 4, and is explored in more detail in an analysis of the bivariate Hα/M_r LF in Gunawardhana et al. (in preparation).

Finally, the Hα luminosity density at a given Hα luminosity is given by

$$\rho_{\rm H\alpha}(L) = L_{\rm H\alpha} \times \Phi(L). \quad (12)$$

The luminosity density versus luminosity distributions are shown in Fig. 14. The peak luminosity density occurs approximately at L^*, demonstrating both that it is typically galaxies close to L^* that dominate the luminosity density of the universe at low redshift, and also the modest evolution in Hα luminosity density with redshift. Although not shown in Fig. 14, the best-fitting L^* values from the Schechter functional fits to the LFs are always larger than those corresponding to the Saunders fits. GAMA and SDSS LFs indicate a Gaussian-like decrease in number density with increasing luminosity owing to the large range in luminosity sampled. Therefore,

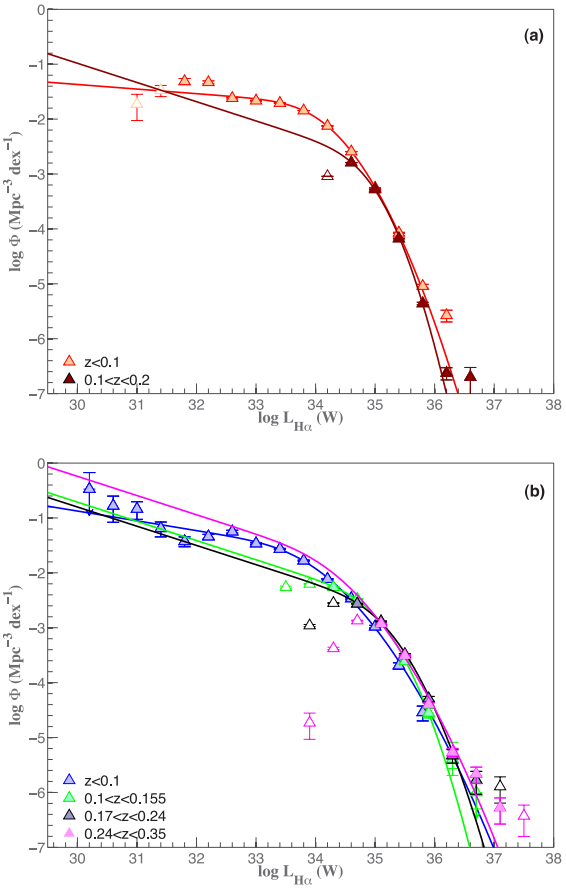

Figure 13. A comparison of GAMA (a) and SDSS (b) Hα LFs, and their functional fits, demonstrating the modest evolution over the observed redshift range. Again, the colour scheme corresponds to that from Fig. 11.

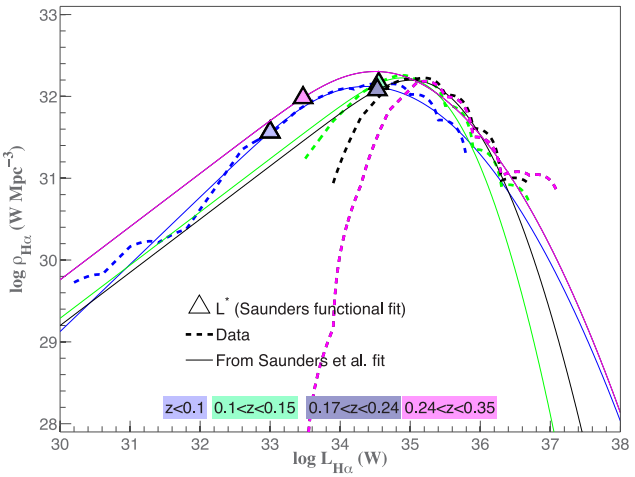

Figure 14. The Hα luminosity density as a function of Hα luminosity, and its evolution. This illustrates that the bulk of the luminosity density comes from galaxies with luminosities close to L^*. The solid lines indicate the luminosity densities derived from the Saunders fits shown in Figs 11 and 13, and dashed lines indicate luminosity densities derived directly from the data. The solid symbols indicate L^* values obtained from Saunders (triangles; best-fitting L^*, log C, α and σ are estimated for the lowest-z LF, α is fixed to be -1.35 and the best-fitting L^*, log C and σ are estimated for the rest). Note that the best-fitting L^* values corresponding to a Saunders functional fit are smaller than that obtained from a Schechter functional fit.

fitting a Schechter function to our data is clearly not appropriate, and results in an overestimation of L^*, see Fig. 12. This is discussed further in Appendix A, and illustrated in Fig. A4.

6 THE COSMIC HISTORY OF STAR FORMATION

The cosmic SFH is a fundamental component in understanding galaxy formation and evolution. The observed SFH encompasses the imprint of all the underlying physical processes such as mergers, feedback processes, accretion, etc. that shape a galaxy, and is a crucial constituent in constraining galaxy formation/evolution models (e.g. Hopkins & Beacom 2006).

Fig. 15 shows the derived SFRDs from Hα luminosities for the GAMA and SDSS-DR7 samples, compared against a variety of published measurements derived from SFR-sensitive emission lines (Hα, Hβ, [O III] λ5007, [O II] λ3727). Where necessary the data are corrected to the cosmology assumed in this paper using the approach of Hopkins (2004). If the published measurements do not already correct for obscuration, we apply a simple correction assuming one magnitude extinction in Hα. The tables in Appendix A list the published data used in this study.

The GAMA SFRD estimate for the $0.001 < z < 0.1$ range is in agreement with the results Nakamura et al. (2004). They have used optically selected and morphology-classified bright galaxies from the SDSS northern stripe to estimate SFRD at $z \sim 0.1$. We should expect to see an increase in the SFRD over the redshift range probed by GAMA. The GAMA data, shown as filled light blue stars in Fig. 15, however, indicate essentially no evolution in SFRD. These SFRDs correspond to the completeness corrected LFs shown in Fig. 7, with the blue circles indicating the reduction in SFRD if no completeness correction is applied to the LFs. The lack of evolution in SFRD we see is mainly due to the bivariate selection effects discussed in Section 4.3. The SFRD measurements corresponding to $z < 0.1$ GAMA LF (Fig. 11) and $0.1 < z < 0.15$ GAMA LF combined with Gilbank et al. (2010) LF points (Fig. 12) indicate some evolution. This dictates that normalizing GAMA LFs to narrow-band or other magnitude-limited LF data provide a better estimate of the faint-end of the LF, thus increasing the reliability of the final measurement. However, none of the GAMA higher-z LFs normalized to narrow-band LF data indicate any evolution. This is a direct result of the bivariate selection introducing a significant incompleteness to $L > L^*$ LF points (see Section 4.3 and Fig. 9). We see a similar lack of evolution in higher-z SFRD measurements (i.e. the two higher-z data points, see Table B1) from Westra et al. (2010). This is likely due bivariate sample selection as their sample is also drawn from a magnitude-limited survey. The other data points in Fig. 15 indicate the emission-line estimates of SFRDs at different epochs. Emission-line measurements, as direct indicators of on-going star formation in a galaxy, are ideally the best tracers of the evolution of SFRD, and yet this figure shows considerable scatter, almost an order of magnitude, between different surveys.

Despite the spread in SFRDs due to different indicators, the scatter is still present within the SFRDs estimated from individual indicators, in particular Hα emission. Part of this scatter can be explained by the inconsistencies between and biases within the different samples. For instance, most of the data shown here are mainly from narrow-band filter, Hα imaging and broad-band

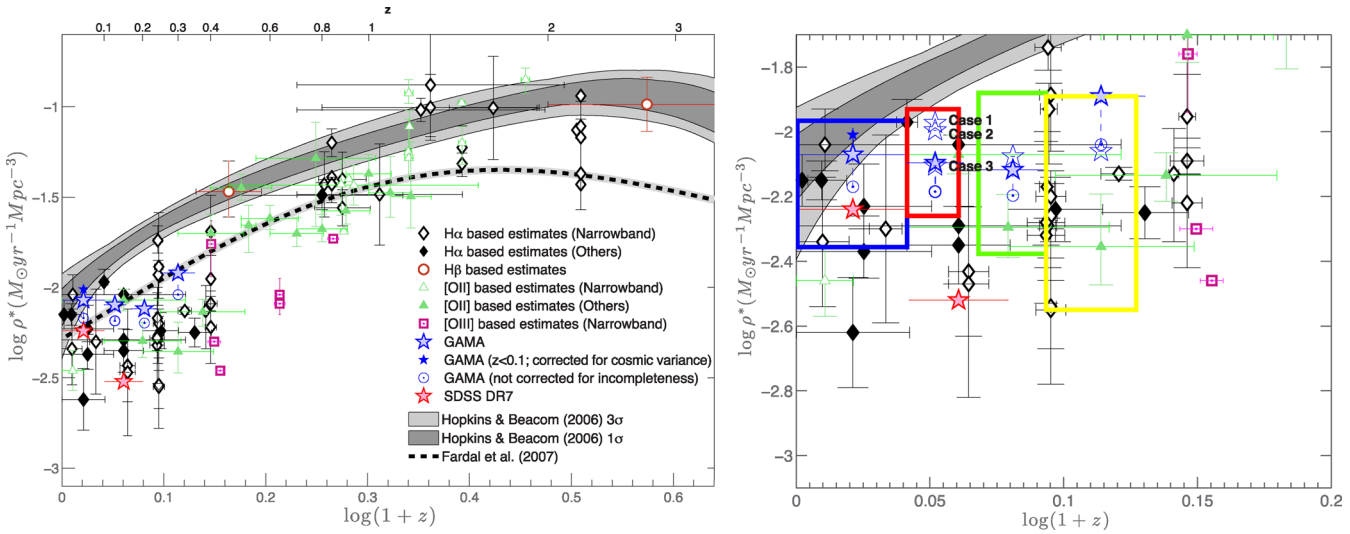

Figure 15. The cosmic history of star formation. The SFRDs estimated using GAMA and SDSS-DR7 Hα LFs are shown as blue and red stars. The filled light blue stars denote the completeness-corrected GAMA SFRDs corresponding to the LFs shown in Fig. 11, with the blue open circles indicating the drop in SFRD if no correction is applied (see Fig. A2 for the LFs). The dark blue filled star indicates the $z < 0.1$ SFRD corrected for GAMA's known underdensity (Driver et al. 2011). The GAMA and SDSS points are compared with other narrow-band/slitless spectroscopy (open symbols) and magnitude-limited and other types (filled symbols) surveys using Hα (black symbols), Hβ (brown), [O II] λ3727 (green) and [O III] λ5007 (magenta). A compilation of published SFRD measurements shown is presented in Appendix B. The shaded regions and the dashed line denote the best-fitting cosmic SFRs derived by Hopkins & Beacom (2006) and Fardal et al. (2007), respectively, using available observational data. All comparisons presented here assume concordance cosmology, and the SFR calibration given in equation (3). The right-hand panel shows zoomed-in comparison. The boxes that bracket the GAMA SFRDs indicate the uncertainties associated with the measurements. The lower/upper edges of the boxes indicate the lower/upper SFRD limits described in Section 4.4 and shown in Fig. 11. Note that these limits, particularly the lower limits, are limits obtained by intentionally calculating unrealistically extreme bounds for the LFs. The overlap between the highest-z SFRD point and the upper limit (yellow box) is due to the functional fit to the LF data being overestimated. This is a result of the small number of LF data that can be used for the functional fitting as the highest-z LF becomes incomplete (i.e. turns over) at luminosities $>L^*$. The open blue stars in the right-hand panel indicate the SFRD measurements calculated by combining higher-z GAMA LFs with other LFs in the literature. The combined LFs and their functional fits are shown in Fig. 12 and the best-fitting parameters are given in Table 3. The three entries for $0.1 < z < 0.15$ given in Table 3 are shown as case 1 (dashed green line in Fig. 12), 2 (solid green line in Fig. 12) and 3 (dot–dashed black line in Fig. 12).

magnitude-selected surveys. The spectroscopy of optically selected emission-line samples is biased by the bivariate selection discussed in Section 4.3. As such, a galaxy sample drawn from a magnitude-selected survey tends to be incomplete. Narrow-band filter surveys, although not subject to this effect, suffer from cosmic (sample) variance issues, uncertainties due to dust corrections, and the blending of Hα and [N II] in narrow-band filters, unless spectroscopic data are available (e.g. López-Sánchez & Esteban 2008). Such surveys are currently limited in area to at most few square degrees, and consequently are only able to probe a narrow range in the LF, e.g. log $L_{\rm H\alpha} \approx 31-33$ (W) over $z \approx 0.065-0.095$ (Ly et al. 2007) and log $L_{\rm H\alpha} \approx 32.5-33.5$ (W) over $z \approx 0.08$ (Jones & Bland-Hawthorn 2001). At high redshifts, narrow-band surveys are more complete as they become less sensitive to cosmic (sample) variance, reducing the scatter in SFRD measurements at these redshifts.

In view of the biases introduced into our sample through differences in survey selection criteria, the local SFH measured by GAMA (blue stars) is a lower limit. Nonetheless, GAMA provides currently the best galaxy sample to investigate star formation in the local universe, and therefore (currently) the best estimates of the SFRDs at low-z. The SFRDs at higher redshift ranges are underestimated as a result of the joint selection imposed on our GAMA star-forming sample. As we showed in Section 4.3, this incompleteness is a result of drawing a star-forming galaxy sample from a magnitude-limited survey, introducing a bias to the sample against optically faint star-forming systems.

The SFHs of Hopkins & Beacom (2006), the best-fitting to far-ultraviolet (FUV) and IR observational data, and Fardal et al. (2007), the best-fitting to UV, emission-line and IR observational data, are also shown in Fig. 15. Most of the low-redshift ($z \lesssim 1$) FUV SFRD estimates used by Hopkins & Beacom (2006) are based on u-band luminosity, a reasonable alternative to FUV luminosity (Hopkins et al. 2003). Also, the u-band luminosity has two advantages over FUV, the availability of more data for better statistics, and being less affected by extinction (Prescott et al. 2009). In this context, the u-band luminosity has the additional advantage of not being subject to a bivariate selection. For these reasons, the Hopkins & Beacom (2006) SFH is likely somewhat more complete than both emission-line-based measurements and the Fardal et al. (2007) SFH. This is consistent with the emission-line-based measurements being on average lower than those from the combination of UV and IR.

The sensitivity of various star formation indicators to different time-scales must also be considered. Emission-line indicators are sensitive to shorter time-scales of typically $\leq$10 Myr than UV estimators, $\geq$100 Myr–1 Gyr (Moustakas, Kennicutt & Tremonti 2006; Gilbank et al. 2010; Koribalski & López-Sánchez 2009; López-Sánchez et al. 2012). u-band measures are likely contaminated by the flux from old stellar populations, and consequently caution must be used in order not to overestimate the derived SFRDs (Cram et al. 1998; Kennicutt 1998; Hopkins et al. 2003), although an u-band–SFR relationship seems to be valid for starburst galaxies (López-Sánchez 2010).

6.1 Impact of the assumptions on cosmic SFH

A number of assumptions are made in order to calculate the SFRDs presented in this paper. Here, we summarize the impact of some of those assumptions on the cosmic SFRD.

In Section 4.4.1, we discuss how the LF varies if the assumed Hα flux limit is varied. That analysis indicates that the change in L^* can be as much as $\sim$0.4 dex if we increase our assume $F_{H\alpha}$ limit to 3×10^{-18} W m^{-2}. While this may seem like a significant effect, this change introduces only an $\sim$10 per cent variation to the integrated SFRD.

The Balmer line measurements for the GAMA sample are corrected for the underlying stellar absorption by assuming a constant correction (see Section 3). The impact of this assumption on the shape of the LFs is discussed in Section A1.1, the effect on SFRD is minimal.

The uncertainties arising from the completeness corrections (see Section 4) are investigated in Section A1.2 by constructing the LFs without applying any corrections for incompleteness. Fig. 15 shows how the SFRDs would be underestimated if no corrections for incompleteness are applied.

7 COSMIC (SAMPLE) VARIANCE

Cosmic (sample) variance has been widely cited as a prominent contributor to the scatter present between published LF/SFRD measurements (Ly et al. 2007; Westra & Jones 2008), see also Figs 7 and 15. Several authors (Somerville et al. 2004; Driver & Robotham 2010; Moster et al. 2011) have provided prescriptions on addressing cosmic (sample) variance issues.

Driver et al. (2011) and Driver & Robotham (2010) provide a quantitative description of sample variance issues related to the GAMA survey. In short, the three GAMA fields overall are 15 per cent underdense compared to a 5000 deg^2 region of SDSS-DR7 for z out to 0.1. Beyond $z > 0.1$, an internal comparison between the three fields indicates that the cosmic (sample) variance is significant between the fields with the GAMA-09h field being particularly underdense. Table 2 of Driver & Robotham (2010) provides the cosmic (sample) variance values for GAMA over several redshift intervals. Using their method, we estimate cosmic (sample) variance values for the redshift ranges corresponding to the LFs presented in this paper (Table 4). Although the cosmic (sample) variance is significant per GAMA field, it is largely mitigated overall as the sampling variance is inversely related to the number of distinct fields observed.

Given the large sample size and the GAMA observations of three independent fields, we are well placed to investigate the effects of cosmic (sample) variance on star-forming galaxy LFs. The Hα LFs in each redshift bin are generated for each GAMA field (Fig. 16).

Table 4. Sampling variance estimates for GAMA in redshift ranges considered in this study. These estimates are based on the prescription of Driver & Robotham (2010).

z range	Sampling variance (per cent)	Sampling variance per field (per cent)
$0 < z < 0.1$	15	26
$0.1 < z < 0.155$	12	21
$0.17 < z < 0.24$	8	14
$0.24 < z < 0.35$	6	10

The three insets in each panel show the distribution of SFR for galaxies contributing to the three LFs. The underdensity of sources in the GAMA-09h field is clearly evident in the SFR distributions, and from the LFs and their best-fittting Saunders functional forms shown in the first panel (see Table 5 for the best-fitting functional parameters). This local structure is also identified and explored by Driver et al. (2011).

The sampling variance for each field given in Table 4 is an overall estimate of cosmic (sample) variance for the redshift range considered. These estimates translated to uncertainties are small compared to the Poisson errors. This is not to say the effect of large-scale structure is negligible, but the impact of such effects is most significant at low-z. An error based on overall sampling variance over a relatively large redshift range does not necessarily represent the large-scale effect influencing the faint-end of the LF. Instead, we estimate a cosmic (sample) variance error for each LF data point, using the Driver & Robotham (2010) prescription. These uncertainties, shown as black error bars in Fig. 16, are only indicative and subject to the limitations described in Driver & Robotham (2010). These have a measurable effect only at the lowest luminosity end of the lowest redshift bin.

Finally, we have explored the dispersion in low-redshift ($z < 0.1$) SFRD measurements that may arise from cosmic (sample) variance effects by dividing two GAMA regions, GAMA-09h (a known underdense region) and GAMA-12h (the deepest GAMA field) into eight separate regions each 12 deg^2, and calculating LFs and corresponding SFRDs for each of the sub-region. This provides a direct indication of the significance of cosmic (sample) variance as we are comparing LFs and SFRDs estimated using a single data set. In other words, the SFRDs corresponding to the 12 sub-regions are not influenced by the assumptions about different surveys, measurements and corrections.

The results indicate that the dispersion between measurements due to cosmic (sample) variance at low redshift can be as large as 0.4 dex. The SFRDs estimated from the LFs constructed from the four sub-regions within GAMA-09h field, a known underdense field, indicate the largest variation. The results of this analysis highlight that a survey covering a large sky area (greater than 12 deg^2) is needed to reduce the non-negligible influence of cosmic (sample) variance.

8 SUMMARY

We have used large samples of GAMA and SDSS galaxies covering a wide range in SFR to construct the Hα LFs in several redshift bins. Owing to the deep spectroscopic observations of GAMA combined with the area of the survey, both the faint and bright ends of the low-redshift ($z < 0.1$) star-forming LF are explored in detail in this study.

The key results are as follows.

(i) The Saunders et al. (1990) functional form, which is used to fit the observed radio and far-infrared LFs for star-forming galaxies in the literature, now proves to be a good representation of the Hα LF. This is an important result demonstrating that a consistent functional form reproduces the LF of the star-forming galaxies at a variety of different SFR-sensitive wavelengths.

(ii) Using GAMA data, we extend the observed Hα LF by approximately one order of magnitude in luminosity towards both fainter and brighter luminosities than other published results. The low-z GAMA and SDSS LFs indicate an increasing number density of star-forming galaxies at faint luminosities. While this result

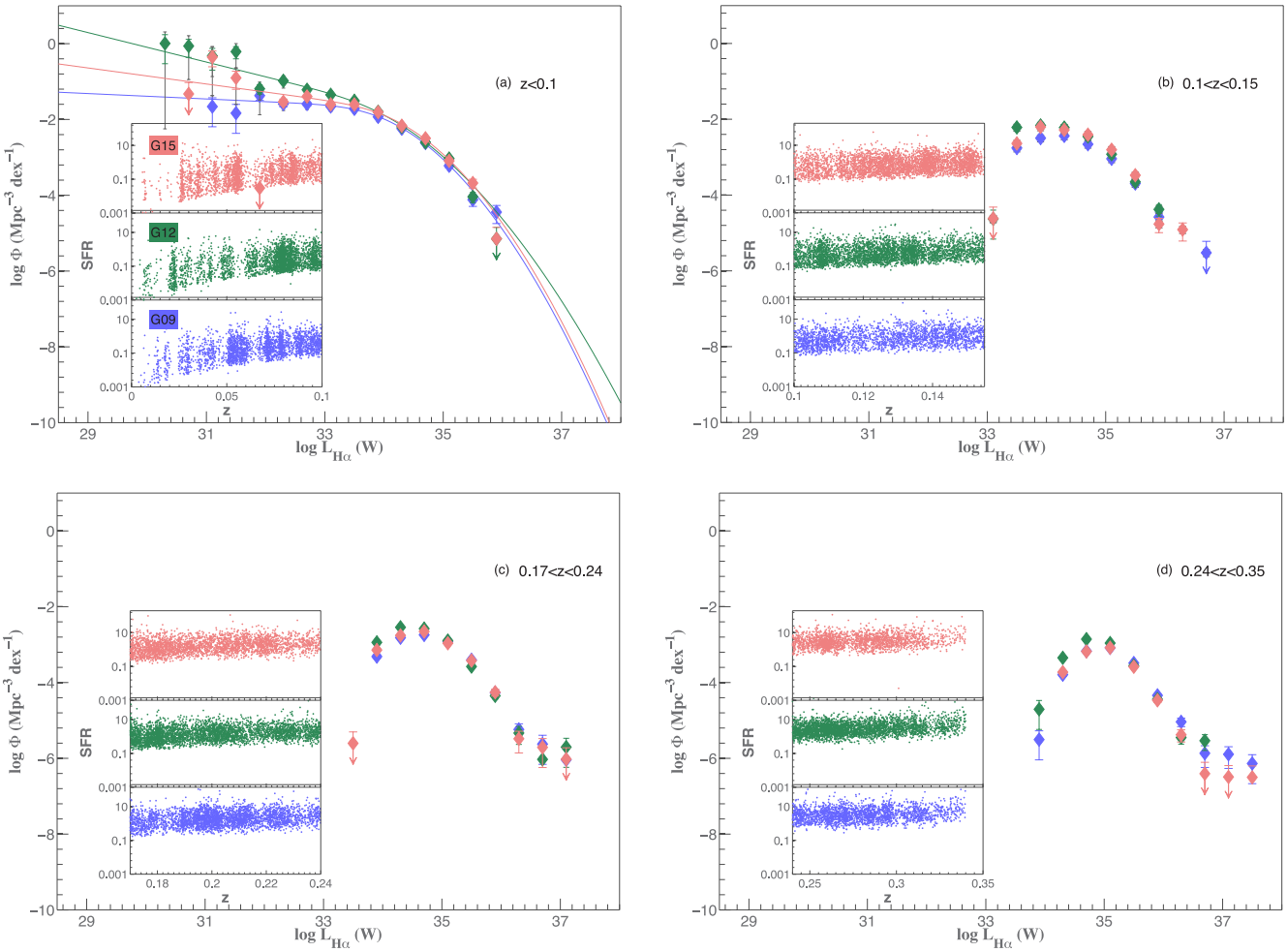

Figure 16. The observations of three independent fields, and the availability of a large number of galaxies gives an opportunity to investigate the effects of cosmic (sample) variance on the star-forming LFs. Hα LFs of each GAMA field in four redshift bins. The error bars shown in black, which are mostly smaller than the Poisson errors, correspond to the cosmic (sample) variance estimates. The insets in each panel show the distribution of SFR of galaxies in each GAMA field over the redshift range considered.

Table 5. The best-fitting Saunders parameters for the $z < 0.1$ LFs in the three independent GAMA fields.

GAMA field	log L^* (W)	log C	α	σ
GAMA-09h	33.14 ± 0.49	-1.97 ± 0.17	-1.07 ± 0.13	0.76 ± 0.10
GAMA-12h	33.12 ± 1.07	-1.66 ± 0.61	-1.38 ± 0.15	0.91 ± 0.28
GAMA-15h	33.39 ± 1.06	-1.93 ± 0.42	-1.21 ± 0.16	0.75 ± 0.30

is qualitatively in agreement with the LFs of Westra et al. (2010) and James et al. (2008), we observe this effect at fainter luminosities than they reach. The nature of this faint population has been examined further in Brough et al. (2011).

(iii) We investigate the effects of bivariate selection and find that it introduces an incompleteness that is difficult to account for, excluding optically faint but Hα bright systems. We find that the SFRD estimates from emission-line measures are affected strongly by bivariate selection, leading to the large scatter seen in the SFH.

(iv) We have investigated the comic (sample) variance effects on GAMA LFs by dividing two GAMA regions (GAMA-09h and GAMA-12h) into 12 deg^2 regions, and calculating LFs and SFRDs for each sub-region. We find that the dispersion in SFRDs due to cosmic (sample) variance can be between factors of 2–3.

(v) We exhaustively test a number of potential biases, systematics and limitations such as the assumption of a constant stellar absorption and completeness corrections, the empirical estimation of BDs, cosmic (sample) variance issues, etc., on the calculation of the LFs, and find that our results are robust to all of these.

(vi) The bivariate M_r/Hα selection imposed on the GAMA and SDSS emission-line galaxies make the star-forming samples somewhat incomplete. As a consequence, the SFRDs we derive can only be lower limits. Nonetheless, our measurements are the best

estimates to date of the low-redshift Hα LFs, and the corresponding luminosity density arising from Hα.

ACKNOWLEDGEMENTS

We thank Russell Jurek and Eduard Westra for valuable discussions. We also thank the anonymous referee for extensive comments that have helped to refine our analysis and discussion.

GAMA is a joint European-Australasian project based around a spectroscopic campaign using the Anglo-Australian Telescope. The GAMA input catalogue is based on data taken from the SDSS and the UKIRT Infrared Deep Sky Survey. Complementary imaging of the GAMA regions is being obtained by a number of independent survey programmes including *GALEX* MIS, VST KIDS, VISTA VIKING, *WISE*, *Herschel*-ATLAS, GMRT and ASKAP providing UV to radio coverage. GAMA is funded by the STFC (UK), the ARC (Australia), the AAO and the Participating Institutions. The GAMA website is http://www.gama-survey.org/.

Funding for the SDSS and SDSS-II has been provided by the Alfred P. Sloan Foundation, the Participating Institutions, the National Science Foundation, the US Department of Energy, the National Aeronautics and Space Administration, the Japanese Monbukagakusho, the Max Planck Society and the Higher Education Funding Council for England. The SDSS website is http://www.sdss.org/.

The SDSS is managed by the Astrophysical Research Consortium for the Participating Institutions. The Participating Institutions are the American Museum of Natural History, Astrophysical Institute Potsdam, University of Basel, University of Cambridge, Case Western Reserve University, University of Chicago, Drexel University, Fermilab, the Institute for Advanced Study, the Japan Participation Group, Johns Hopkins University, the Joint Institute for Nuclear Astrophysics, the Kavli Institute for Particle Astrophysics and Cosmology, the Korean Scientist Group, the Chinese Academy of Sciences (LAMOST), Los Alamos National Laboratory, the Max-Planck-Institute for Astronomy (MPIA), the Max-Planck-Institute for Astrophysics (MPA), New Mexico State University, Ohio State University, University of Pittsburgh, University of Portsmouth, Princeton University, the United States Naval Observatory and the University of Washington.

MLPG acknowledges support provided through the Australian Postgraduate Award and Australian Astronomical Observatory PhD scholarship. JL acknowledges support from the Science and Technology Facilities Council (grant number ST/I000976/1).

REFERENCES

Abazajian K. N. et al., 2009, ApJS, 182, 543
Adelman-McCarthy J. K. et al., 2008, ApJS, 175, 297
Afonso J., Hopkins A., Mobasher B., Almeida C., 2003, ApJ, 597, 269
Baldry I. K., Glazebrook K., 2003, ApJ, 593, 258
Baldry I. K. et al., 2010, MNRAS, 404, 86
Baldry I. K. et al., 2012, MNRAS, 421, 621
Baldwin J. A., Phillips M. M., Terlevich R., 1981, PASP, 5, 93 (BPT)
Bastian N., Covey K. R., Meyer M. R., 2010, AR&A, 48, 339
Bayliss K. D., McMahon R. G., Venemans B. P., Ryan-Weber E. V., Lewis J. R., 2011, MNRAS, 413, 2883
Best P. N., Kauffmann G., Heckman T. M., Brinchmann J., Charlot S., Ivezić Ž., White S. D. M., 2005, MNRAS, 362, 25
Blanton M. R., Roweis S., 2007, AJ, 133, 734
Blanton M. R. et al., 2003, ApJ, 592, 819
Blanton M. R., Lupton R. H., Schlegel D. J., Strauss M. A., Brinkmann J., Fukugita M., Loveday J., 2005, ApJ, 631, 208
Blanton M. R. et al., 2005, AJ, 129, 2562
Bouwens R. J. et al., 2010, ApJ, 709, L133
Bouwens R. J. et al., 2011, Nat, 469, 504
Brinchmann J., Charlot S., White S. D. M., Tremonti C., Kauffmann G., Heckman T., Brinkmann J., 2004, MNRAS, 351, 1151
Brough S. et al., 2011, MNRAS, 413, 1236
Bruzual G., Charlot S., 2003, MNRAS, 344, 1000
Cardelli J. A., Clayton G. C., Mathis J. S., 1989, in Allamandola L. J., Tielens A. G. G. M., eds, Proc. IAU Symp. 135, Interstellar Dust. Kluwer, Dordrecht, p. 5
Chary R.-R., 2008, ApJ, 680, 32
Cid Fernandes R., Stasińska G., Schlickmann M. S., Mateus A., Vale Asari N., Schoenell W., Sodré L., 2010, MNRAS, 403, 1036
Cowie L. L., Songaila A., Barger A. J., 1999, AJ, 118, 603
Cram L., Hopkins A., Mobasher B., Rowan-Robinson M., 1998, ApJ, 507, 155
Dale D. A. et al., 2008, AJ, 135, 1412
Dale D. A. et al., 2010, ApJ, 712, L189
Davé R., 2011, in Treyer M., Wyder T., Neill J., Seibert M., Lee J., eds, ASP Conf. Ser. Vol. 440, UP2010: Have Observations Revealed a Variable Upper End of the Initial Mass Function? Astron. Soc. Pac., San Francisco, p. 35
De Propris R., Conselice C. J., Liske J., Driver S. P., Patton D. R., Graham A. W., Allen P. D., 2007, ApJ, 666, 212
Doherty M., Bunker A., Sharp R., Dalton G., Parry I., Lewis I., 2006, MNRAS, 370, 331
Dressler A., Oemler A., Gladders M. G., Bai L., Rigby J. R., Poggianti B. M., 2009, ApJ, 699, L130
Driver S. P., Robotham A. S. G., 2010, MNRAS, 407, 2131
Driver S. P. et al., 2009, Astron. Geophys., 50, 5
Driver S. P. et al., 2011, MNRAS, 413, 971
Dutton A. A. et al., 2011, MNRAS, 416, 322
Fabbiano G., 2005, AR&A, 44, 323
Fardal M. A., Katz N., Weinberg D. H., Davé R., 2007, MNRAS, 379, 985
Feulner G., Gabasch A., Salvato M., Drory N., Hopp U., Bender R., 2005, ApJ, 633, L9
Fujita S. S. et al., 2003, ApJ, 586, L115
Gallego J., Zamorano J., Aragon-Salamanca A., Rego M., 1995, ApJ, 455, L1
Gallego J., García-Dabó C. E., Zamorano J., Aragón-Salamanca A., Rego M., 2002, ApJ, 570, L1
Geach J. E., Smail I., Best P. N., Kurk J., Casali M., Ivison R. J., Coppin K., 2008, MNRAS, 388, 1473
Georgakakis A., Hopkins A. M., Sullivan M., Afonso J., Georgantopoulos I., Mobasher B., Cram L. E., 2003, MNRAS, 345, 939
Gerssen J., Wilman D. J., Christensen L., 2012, MNRAS, 420, 197
Gilbank D. G., Baldry I. K., Balogh M. L., Glazebrook K., Bower R. G., 2010, MNRAS, 405, 2594
Glazebrook K., Blake C., Economou F., Lilly S., Colless M., 1999, MNRAS, 306, 843
Glazebrook K., Tober J., Thomson S., Bland-Hawthorn J., Abraham R., 2004, AJ, 128, 2652
Gunawardhana M. L. P. et al., 2011, MNRAS, 415, 1647
Gunn J. E. et al., 1998, AJ, 116, 3040
Haarsma D. B., Partridge R. B., Windhorst R. A., Richards E. A., 2000, ApJ, 544, 641
Hammer F. et al., 1997, ApJ, 481, 49
Hanish D. J. et al., 2006, ApJ, 649, 150
Hayes M., Schaerer D., Östlin G., 2010, A&A, 509, L5
Hill D. T. et al., 2011, MNRAS, 412, 765
Hippelein H. et al., 2003, A&A, 402, 65
Hogg D. W., Cohen J. G., Blandford R., Pahre M. A., 1998, ApJ, 504, 622
Hopkins A. M., 2004, ApJ, 615, 209
Hopkins A. M., Beacom J. F., 2006, ApJ, 651, 142
Hopkins A. M., Mobasher B., Cram L., Rowan-Robinson M., 1998, MNRAS, 296, 839
Hopkins A. M., Connolly A. J., Szalay A. S., 2000, AJ, 120, 2843
Hopkins A. M., Connolly A. J., Haarsma D. B., Cram L. E., 2001, AJ, 122, 288

Hopkins A. M. et al., 2003, ApJ, 599, 971
Hopkins A. M., McClure-Griffiths N. M., Gaensler B. M., 2008, ApJ, 682, L13
Hopkins A. M. et al., 2013, MNRAS, 430, 2047
Hoversten E. A., Glazebrook K., 2008, ApJ, 675, 163
James P. A. et al., 2004, A&A, 414, 23
James P. A., Knapen J. H., Shane N. S., Baldry I. K., de Jong R. S., 2008, A&A, 482, 507
Jones D. H., Bland-Hawthorn J., 2001, ApJ, 550, 593
Juneau S. et al., 2005, ApJ, 619, L135
Karachentsev I. D., Kaisin S. S., 2010, AJ, 140, 1241
Kauffmann G. et al., 2003, MNRAS, 346, 1055
Kennicutt R. C., Jr, 1998, ARA&A, 36, 189
Kereš D., Katz N., Weinberg D. H., Davé R., 2005, MNRAS, 363, 2
Kewley L. J., Dopita M. A., Sutherland R. S., Heisler C. A., Trevena J., 2001, ApJ, 556, 121
Kewley L. J., Groves B., Kauffmann G., Heckman T., 2006, MNRAS, 372, 961
Kistler M. D., Yüksel H., Beacom J. F., Hopkins A. M., Wyithe J. S. B., 2009, ApJ, 705, L104
Koribalski B. S., López-Sánchez Á. R., 2009, MNRAS, 400, 1749
Le Fèvre O. et al., 2000, MNRAS, 311, 565
Lilly S. J., Le Fevre O., Hammer F., Crampton D., 1996, ApJ, 460, L1
López-Sánchez Á. R., 2010, A&A, 521, 63
López-Sánchez Á. R., Esteban C., 2008, A&A, 491, 131
López-Sánchez A. R., Esteban C., 2009, A&A, 508, 615
López-Sánchez Á. R., Koribalski B. S., van Eymeren J., Esteban C., Kirby E., Jerjen H., Lonsdale N., 2012, MNRAS, 419, 1051
Lotz J. M. et al., 2008, ApJ, 672, 177
Lotz J. M., Jonsson P., Cox T. J., Croton D., Primack J. R., Somerville R. S., Stewart K., 2011, ApJ, 742, 103
Loveday J., Peterson B. A., Efstathiou G., Maddox S. J., 1992, ApJ, 390, 338
Loveday J. et al., 2012, MNRAS, 420, 1239
Ly C. et al., 2007, ApJ, 657, 738
Ly C., Lee J. C., Dale D. A., Momcheva I., Salim S., Staudaher S., Moore C. A., Finn R., 2011, ApJ, 726, 109
Madau P., Ferguson H. C., Dickinson M. E., Giavalisco M., Steidel C. C., Fruchter A., 1996, MNRAS, 283, 1388
Massarotti M., Iovino A., Buzzoni A., 2009, ApJ, 559, L105
Meurer G. R. et al., 2009, ApJ, 695, 765
Mobasher B. et al., 2009, ApL, 690, 1074
Moorwood A. F. M., van der Werf P. P., Cuby J. G., Oliva E., 2000, AAP, 362, 9
Morioka T., Nakajima A., Taniguchi Y., Shioya Y., Murayama T., Sasaki S. S., 2008, PASJ, 60, 1219
Moster B. P., Somerville R. S., Newman J. A., Rix H.-W., 2011, ApJ, 731, 113
Moustakas J., Kennicutt R. C., Jr, Tremonti C. A., 2006, ApJ, 642, 775
Nakamura O., Fukugita M., Brinkmann J., Schneider D. P., 2004, AJ, 127, 2511
Osterbrock D. E., 1989, Astrophysics of Gaseous Nebulae and Active Galactic Nuclei, University Science Books, Mill Valley, CA
Pascual S., 2005, PASP, 117, 120
Pascual S., Gallego J., Aragón-Salamanca A., Zamorano J., 2001, A&A, 379, 798
Pérez-González P. G., Zamorano J., Gallego J., Aragón-Salamanca A., Gil de Paz A., 2003, ApJ, 591, 827
Pérez-González P. G. et al., 2005, ApJ, 630, 82
Pérez-González P. G. et al., 2008, ApJ, 675, 234
Pettini M., Kellogg M., Steidel C. C., Dickinson M., Adelberger K. L., Giavalisco M., 1998, ApJ, 508, 539
Prescott M., Baldry I. K., James P. A., 2009, MNRAS, 397, 90
Reddy N. A., Steidel C. C., 2009, ApJ, 692, 778
Reddy N. A., Steidel C. C., Pettini M., Adelberger K. L., Shapley A. E., Erb D. K., Dickinson M., 2007, ApJS, 175, 48
Robotham A. et al., 2010, Publ. Astron. Soc. Aust., 27, 76
Robotham A. et al., 2013, MNRAS, 431, 167
Rowan-Robinson M., Benn C. R., Lawrence A., McMahon R. G., Broadhurst T. J., 1993, MNRAS, 263, 123
Salim S., Lee J. C., 2012, ApJ, 758, 134
Salpeter E. E., 1955, ApJ, 121, 161
Sarzi M. et al., 2006, MNRAS, 366, 1151
Saunders W., Rowan-Robinson M., Lawrence A., Efstathiou G., Kaiser N., Ellis R. S., Frenk C. S., 1990, MNRAS, 242, 318
Saunders W., Cannon R., Sutherland W., 2004, Anglo-Australian Observatory Epping Newsletter, 106, 16
Schechter P., 1976, ApJ, 203, 297
Schiminovich D. et al., 2005, ApJ, 619, L47
Schlegel D. J., Finkbeiner D. P., Davis M., 1998, ApJ, 500, 525
Schmidt M., 1968, ApJ, 151, 393
Seymour N. et al., 2008, MNRAS, 386, 1695
Sharp R., Parkinson H., 2010, MNRAS, 408, 2495
Sharp R. et al., 2006, in McLean I. S., Masanori I., eds, Proc. SPIE Vol. 6269, Ground-based and Airborne Instrumentation for Astronomy. SPIE, Bellingham, p. 62690G
Shim H., Colbert J., Teplitz H., Henry A., Malkan M., McCarthy P., Yan L., 2009, ApJ, 696, 785
Shioya Y. et al., 2008, ApJS, 175, 128
Sobral D. et al., 2009, MNRAS, 398, 75
Sobral D., Best P. N., Matsuda Y., Smail I., Geach J. E., Cirasuolo M., 2012, MNRAS, 420, 1926
Sobral D. et al., 2013, MNRAS, 428, 1128
Somerville R. S., Lee K., Ferguson H. C., Gardner J. P., Moustakas L. A., Giavalisco M., 2004, ApJL, 600, L171
Spector O., Finkelman I., Brosch N., 2012, MNRAS, 419, 2156
Strauss M. A. et al., 2002, AJ, 124, 1810
Sullivan M., Treyer M. A., Ellis R. S., Bridges T. J., Milliard B., Donas J., 2000, MNRAS, 312, 442
Tadaki K.-I., Kodama T., Koyama Y., Hayashi M., Tanaka I., Tokoku C., 2011, PASJ, 63, 437
Takahashi M. I. et al., 2007, ApJS, 172, 456
Taylor E. N. et al., 2011, MNRAS, 418, 1587
Teplitz H. I., Collins N. R., Gardner J. P., Hill R. S., Rhodes J., 2003, ApJ, 589, 704
Tonry J. L., Blakeslee J. P., Ajhar E. A., Dressler A., 2000, ApJ, 530, 625
Tremonti C. A. et al., 2004, ApJ, 613, 898
Tresse L., Maddox S. J., 1998, ApJ, 495, 691
Tresse L., Maddox S. J., Le Fèvre O., Cuby J.-G., 2002, MNRAS, 337, 369
van de Voort F., Schaye J., Booth C. M., Dalla Vecchia C., 2011, MNRAS, 415, 2782
Villar V., Gallego J., Pérez-González P. G., Pascual S., Noeske K., Koo D. C., Barro G., Zamorano J., 2008, ApJ, 677, 169
Westra E., Jones D. H., 2008, MNRAS, 383, 339
Westra E., Geller M. J., Kurtz M. J., Fabricant D. G., Dell'Antonio I., 2010, ApJ, 708, 534
Wijesinghe D. B. et al., 2011, MNRAS, 410, 2291
Wilkins S. M., Trentham N., Hopkins A. M., 2008a, MNRAS, 385, 687
Wilkins S. M., Hopkins A. M., Trentham N., Tojeiro R., 2008b, MNRAS, 391, 363
Woosley S. E., Bloom J. S., 2006, ARA&A, 44, 507
Xue Y. Q. et al., 2010, ApJ, 720, 368
Yan L., McCarthy P. J., Freudling W., Teplitz H. I., Malumuth E. M., Weymann R. J., Malkan M. A., 1999, ApJ, 519, L47
York D. G. et al., 2000, AJ, 120, 1579
Yüksel H., Kistler M. D., Beacom J. F., Hopkins A. M., 2008, ApJ, 683, L5
Zheng X. Z., Bell E. F., Papovich C., Wolf C., Meisenheimer K., Rix H.-W., Rieke G. H., Somerville R., 2007, ApJ, 661, L41

APPENDIX A: BIASES, SYSTEMATICS AND LIMITATIONS

In this section, we explore a number of potential biases to identify the level of uncertainty they introduce to the LFs, and SFRDs presented in this paper.

A1 Low-SFR galaxies

A1.1 Constant stellar absorption corrections

Brough et al. (2011) investigate the properties of low-luminosity galaxies contributing to the rise in Φ shown in Fig. 7(a). Here, we investigate how the assumption of a constant stellar absorption correction in the derivation of Hα luminosities affects the GAMA low-z LF. Hopkins et al. (2003) argue a stellar absorption correction of 1.3 Å is sufficient. We find that a stellar absorption correction in the range 0.7–1.3 Å for GAMA galaxies in $0 < z < 0.35$ causes a negligible change to the majority of the Hα luminosities and SFRs, although the lowest luminosity systems are the most affected (Gunawardhana et al. 2011). For the analysis presented in this paper, we have assumed a fairly conservative stellar absorption correction of 2.5 Å.

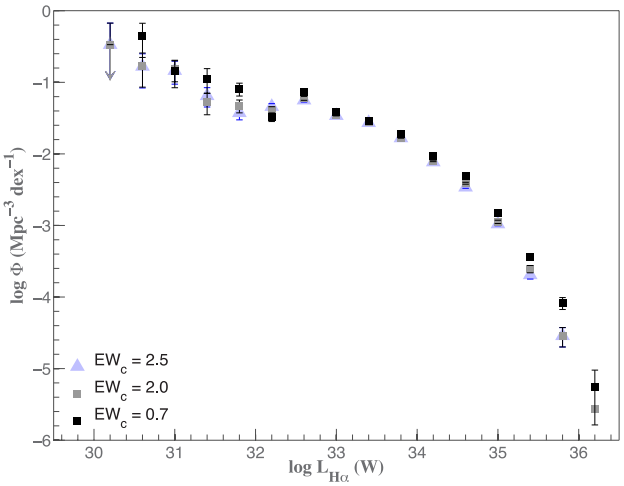

Figure A1. We reproduce the GAMA low-z LF assuming different stellar absorption corrections (EW$_c$ in Å) to investigate how the assumption of a constant EW$_c$ affects the shape of the LF at faint luminosities.

Here, we investigate quantitatively how different stellar absorption corrections affect the low-z LF.

Fig. A1 shows the variation in the GAMA low-z LF if we assume different stellar absorption corrections. We perform this analysis only for the GAMA sample, since the emission-line measurements for SDSS galaxies in GAMA fields are taken from the MPA-JHU data base, which are already corrected for stellar absorption. Also, the SDSS galaxies contributing to the GAMA low-z LF are the bright galaxies in our sample. Typically, any uncertainty arising from stellar absorption corrections affects primarily the lowest Hα luminosity galaxies, and weak line systems. For the lowest-z LF, the assumption of low-EW$_c$ values only affects the faintest end of the Hα LF, and even then only in a modest way. In the case of higher-z LFs, the assumption of low-EW$_c$ values act to increase the integrated SFRD.

A1.2 Uncertainties from completeness corrections

The determination of completeness corrections for each galaxy is described in Section 4. Here, we investigate the effects

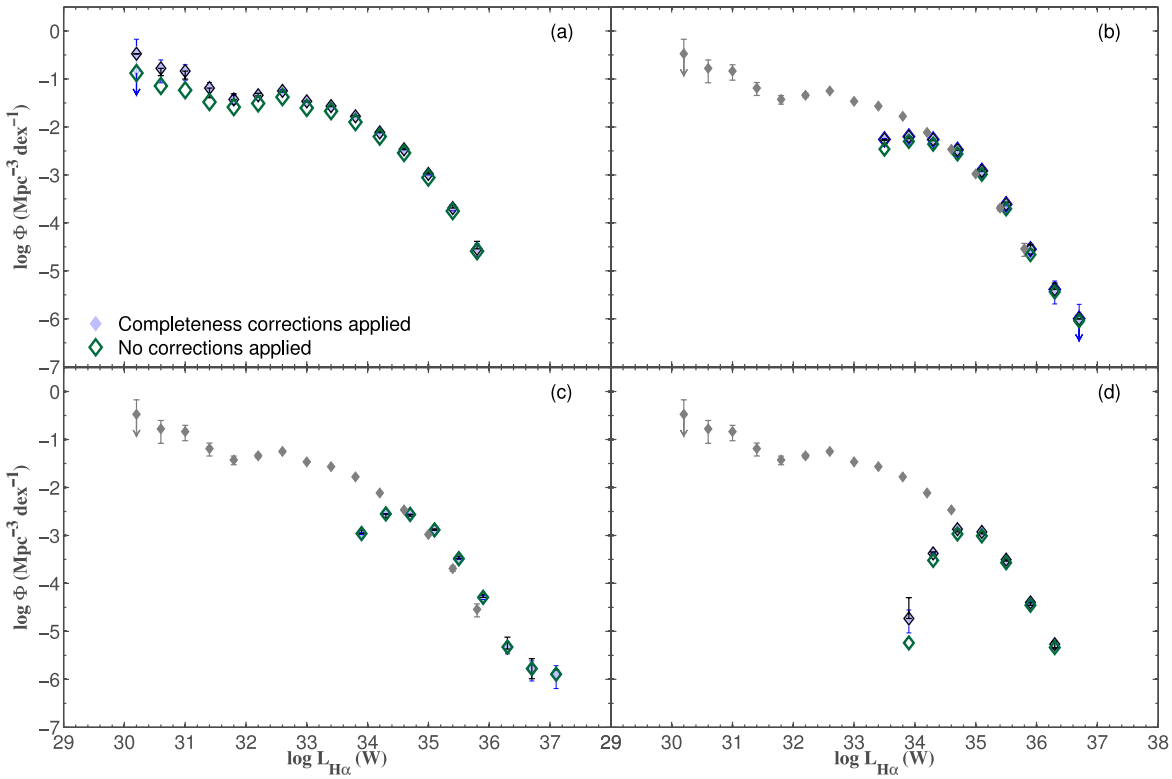

Figure A2. The effects of the completeness correction and the uncertainties arising from the empirical estimation of BDs for galaxies without measured Hβ fluxes are investigated here. The error bars shown in black in each panel are estimated using a Monte Carlo method and show the full range of the values measured, and the Poisson uncertainties are shown in blue. The filled and open symbols in each panel show the LFs with and without completeness corrections respectively. Not surprisingly, the application of completeness corrections has little effect on improving the shape of the GAMA LFs as the survey is >98 per cent complete. Also shown in (b), (c) and (d) is the low-z LF (faint small symbols) for comparison.

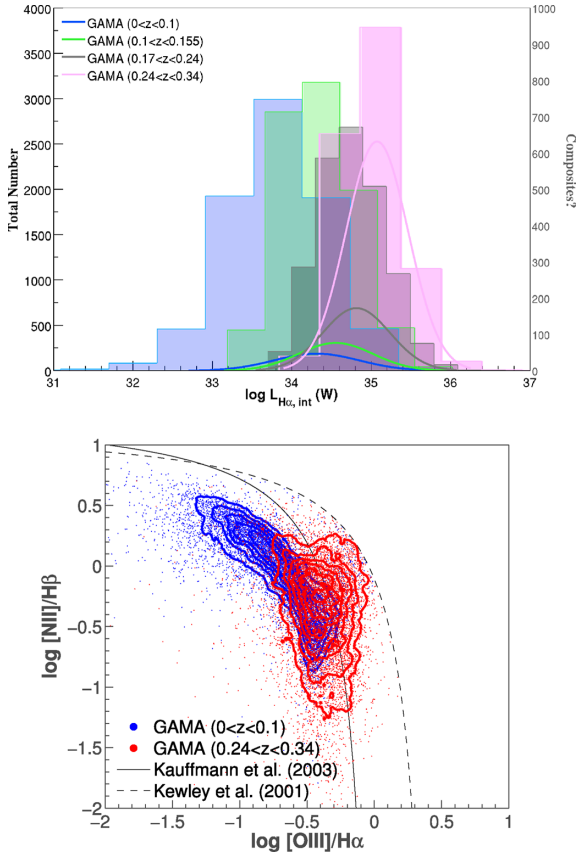

Figure A3. Top panel: the distribution of intrinsic Hα luminosities in four redshift bins compared to the distribution of luminosities of objects classified as composites based on Kauffmann et al. (2003) diagnostic over the same redshift ranges. Bottom panel: the BPT diagnostics for the lowest ($z < 0.1$) and highest ($0.24 < z < 0.34$) redshift samples. The solid line indicates the Kauffmann et al. (2003) relation.

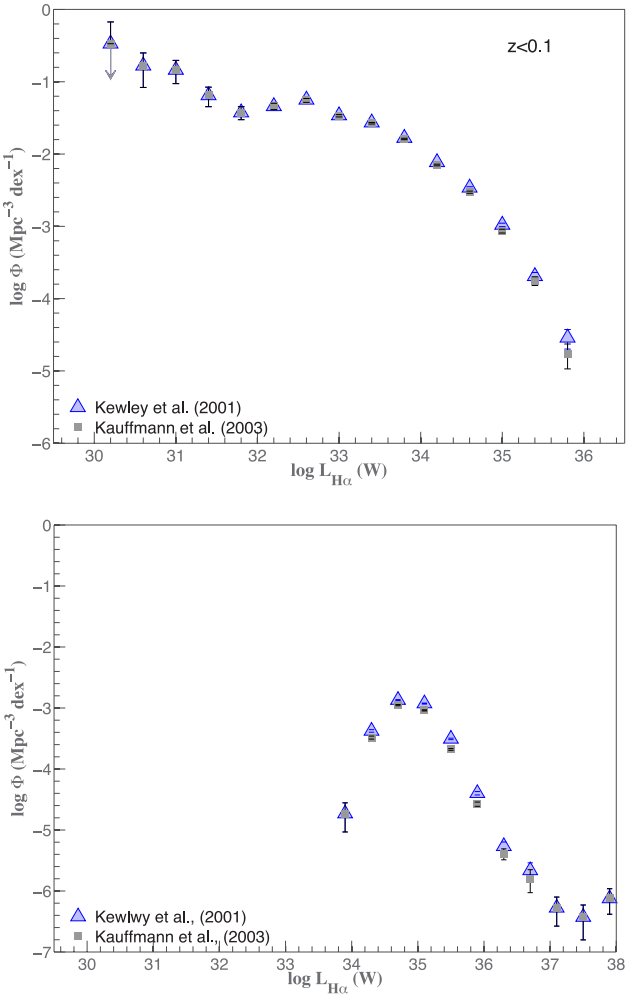

Figure A4. The lowest and highest redshift GAMA LFs shown in Fig. 7 compared to the LFs over the same redshift ranges constructed by excluding objects classified as composites based on Kauffmann et al. (2003) diagnostics (grey points).

of the uncertainties propagated through the application of completeness corrections, and their influence on the shapes of the LFs. A comparison of the LFs before and after the application of completeness corrections (see Fig. A2) indicates that the completeness corrections have a low impact on GAMA LFs. Omitting the correction mostly affects the low-SFR galaxies in each redshift bin. This result is not surprising as the GAMA survey currently has a spectroscopic follow-up completeness of ∼98 per cent, and faint systems are most likely affected by any incompleteness of the survey (Driver et al. 2011; Loveday et al. 2012).

As mentioned before, we have not attempted to apply any completeness corrections to the SDSS-DR7 sample. Nonetheless, based on the GAMA results we assume that the shapes of the SDSS LFs presented in this paper are unlikely to change significantly.

A2 Empirical estimation of BDs

In addition to the examination of the effects of the assumption of a constant stellar absorption correction, we also investigate the effects of empirically estimating BDs for the galaxies without measured Hβ fluxes.

A Monte Carlo experiment is performed using the distribution of BDs as a function of $L_{\mathrm{H}\alpha,\mathrm{ApCor}}$. For each galaxy without a measured BD, rather than assigning it from equation (4), we randomly assign a BD from the observed distribution from galaxies of similar $L_{\mathrm{H}\alpha,\mathrm{ApCor}}$. This process is repeated ∼100 times, and the variation in the resulting LF is indicated by a second set of errors for the LFs. These errors are shown in Fig. A2 in black, the error estimates are simply the highest and the lowest Φ derived in the MC experiment. The uncertainties due to the empirical estimation of BDs becomes more important for high-redshift LFs, as those have the highest fraction of galaxies without Hβ flux measurements. Also, the uncertainties estimated from this analysis for the low-z LF are small both because this z range has the lowest fraction of galaxies without BDs, and the number of galaxies with BDs is particularly low at low $L_{\mathrm{H}\alpha,\mathrm{ApCor}}$ (Fig. 3). Furthermore, the assumption of a flat BD versus $L_{\mathrm{H}\alpha,\mathrm{ApCor}}$ relation above the average luminosity of the sample, for example, resulted in errors smaller than Poisson errors of the sample. Therefore, the effects of the empirical estimation of BDs for the 14 per cent of galaxies without measured Hβ fluxes in the sample are minimal.

A3 AGN contamination

The Kewley et al. (2001) AGN/star-forming diagnostic is used exclude AGNs from the LFs presented in the main paper. Alternatively, the Kauffmann et al. (2003) relation can be used to identify pure

Table B1. Compilation of Hα, Hβ emission-line SFRD measurements

Reference	Redshift (z) (z)	Area (deg^2)	Selection[a]	N[b]	C_1[c]	log $\dot{\rho}_{*,\mathrm{obs}}$[d] ($M_\odot$ yr^{-1} Mpc^{-3})	log $\dot{\rho}_{*,\mathrm{int}}$[e] ($M_\odot$ yr^{-1} Mpc^{-3})
Gallego et al. (1995)	$0 < z < 0.045$	471.40	SLS Hα-selected, UCM	176	1.37	...	-1.91 ± 0.20
Tresse & Maddox (1998)	$0 < z < 0.3$	0.12	*I*-selected, CFRS	138(SF = 110)	1.17	...	-1.61 ± 0.03
Yan et al. (1999)	$0.8 < z < 1.8$	$\sim$0.024	SLS Hα-selected	33	0.837	$-0.96^{+0.09}_{-0.11}$	-0.57 ± 0.18
Sullivan et al. (2000)	$0 < z < 0.3$	$\sim$10	UV-selected, FOCA	216	0.55	...	-1.86 ± 0.06
Tresse et al. (2002)	$0.5 < z < 1.1$	0.12	*I*-selected, CFRS	33	0.88	$-1.37^{+0.07}_{-0.08}$	$-1.06^{+0.07}_{-0.08}$
Fujita et al. (2003)	$0.234 < z < 0.252$	0.2	NBF Hα-selected	348	1.00	$-1.90^{+0.08}_{-0.17}$	$-1.50^{+0.08}_{-0.17}$
Pérez-González et al. (2003)	$0 < z < 0.05$	...	SLS Hα-selected, UCM	79	1.00	...	$-1.61^{+0.11}_{-0.08}$
Nakamura et al. (2004)	$0 < z < 0.12$	229.7	SDSS DR1[f]	1482(SF = 665)	1.00	...	$-1.94^{+0.11}_{-0.082}$
Hippelein et al. (2003)	$0.238 < z < 0.252$	0.1	NBF Hα-selected, CADIS	92	1.00	...	$-1.83^{+0.10}_{-0.13}$
Brinchmann et al. (2004)	$0.09 < z < 0.11$	...	SDSS	...	1.00	...	-1.54 ± 0.07
Westra & Jones (2008)	$0.229 < z < 0.261$	0.262	NBF Hα-selected, CDFS	371	1.00	...	$-1.77^{+0.08}_{-0.10}$ ($-1.93^{+0.08}_{-0.10}$)
	$0.229 < z < 0.261$	0.23	NBF Hα-selected, S11	335	1.00	...	$-2.12^{+0.09}_{-0.12}$ ($-2.24^{+0.11}_{-0.14}$)
Westra et al. (2010)	$0 < z < 0.1$	4	*R*-selected, SHELS	322	1.00	...	-2.19 ± 0.17
	$0.1 < z < 0.2$	"	"	1127	1.00	...	-1.92 ± 0.12
	$0.2 < z < 0.3$	"	"	1268	1.00	...	-1.81 ± 0.10
	$0.3 < z < 0.4$	"	"	848	1.00	...	-1.82 ± 0.08
Westra et al. (2010)	$0.233 < z < 0.251$	4	*R*-selected, SHELS	–	1.00	...	-1.86 ± 0.13
+ Shioya et al. (2008)		+ 1.5	+ NBF Hα-selected	–			
Shioya et al. (2008)	$0.233 < z < 0.249$	1.54	NBF Hα-selected	980	1.00	...	$-1.74^{+0.17}_{-0.097}$
Ly et al. (2007)	$0.065 < z < 0.095$	0.24	NBF Hα-selected	318	1.00		-1.87 ± 0.29
	$0.239 < z < 0.251$	0.24	"	259	1.00	-2.37	-2.11 ± 0.24
	$0.382 < z < 0.418$	0.24	"	391	1.00	-2.10	-1.79 ± 0.20
Hanish et al. (2006)	$0 < z < 0.12$	...	H I-selected, SINGG	110	1.00	...	$-1.80^{+0.13}_{-0.07}$
Geach et al. (2008)	$2.214 < z < 2.246$	0.60	NBF Hα-selected	55	1.00	...	-1.00^{h}
Morioka et al. (2008)	$0.233 < z < 0.251$	0.24+SDSS	NBF Hα-selected + SDSS	575	1.00	...	$-1.456^{+0.3}_{-0.174}$
Villar et al. (2008)	$0.831 < z < 0.849$	0.17	NBF Hα, NIR-selected	165	1.00	-1.009 [α constrained]	-0.77 ± 0.077
Shim et al. (2009)	$0.7 < z < 1.4$	$\sim$0.03	SLS Hα-selected, *HST*-NICMOS	35	1.00		$-1.056^{+0.21}_{-0.44}$
	$1.4 < z < 1.9$	"	"	45	1.00		$-0.577^{+0.22}_{-0.46}$
	$0.7 < z < 1.9$	"	"	80	1.00		$-0.86^{+0.15}_{-0.24}$
Sobral et al. (2009)	$0.829 < z < 0.851$	1.3	NBF Hα-selected, HiZELS	743	1.00	...	-0.96^{g}
Sobral et al. (2012)	$1.45 < z < 1.49$	0.67	NBF, HiZELS	190	1	...	$-0.796^{+0.12}_{-0.16}$
Sobral et al. (2013)	$0.39 < z < 0.41$	2	NBF, HiZELS	1742	1	...	$-1.523^{+0.13}_{-0.18}$
	$0.82 < z < 0.86$	"	"	637	1	...	$-1.00^{+0.04}_{-0.10}$
	$1.45 < z < 1.49$	"	"	515	1	...	$-0.886^{+0.06}_{-0.07}$
	$2.21 < z < 2.25$	"	"	8.7	1	...	$-0.678^{+0.04}_{-0.07}$

Table B1 – *continued*

Reference	Redshift (z) (z)	Area (deg^2)	Selection[a]	N[b]	C_1[c]	log $\dot{\rho}_{*,obs}$[d] ($M_\odot$ yr^{-1} Mpc^{-3})	log $\dot{\rho}_{*,int}$[e] ($M_\odot$ yr^{-1} Mpc^{-3})
Dale et al. (2010)	$0.14 < z < 0.18$	4.19	NBF Hα-selected, WySH	214	1.00	...	$-2.002^{+0.041}_{-0.046}$
	$0.22 < z < 0.26$	4.03	”	424	1.00	...	$-1.89^{+0.032}_{-0.034}$
	$0.30 < z < 0.34$	4.13	”	438	1.00	...	$-1.7^{+0.022}_{-0.021}$
	$0.38 < z < 0.42$	1.11	”	91	1.00	...	$-1.66^{+0.04}_{-0.04}$
Ly et al. (2011)	$0.801 < z < 0.817$	0.82	NBF 1.18 μm-selected NEWFIRM Hα (total sample)	522	1.00	...	-1.00 ± 0.18[h]
	$0.801 < z < 0.817$	0.82	NBF 1.18 μm-selected NEWFIRM Hα ($L \geq L_{lim}$)	414	1.00	...	-1.10 ± 0.09
Hopkins, Connolly & Szalay (2000)	$0.7 < z < 1.8$	0.001	SLS Hα-selected, NICMOS	37	0.57	-0.74	-0.588 ± 0.064
Moorwood et al. (2000)	$2.178 < z < 2.221$	0.028	NBF Hα-selected	10	0.79		-0.70
Glazebrook et al. (1999)	0.885 ± 0.099	0.12	Drawn from I-selected CFRS sample	13	0.89[i]	...	$-0.972^{+0.15}_{-0.14}$[i]
Glazebrook et al. (2004)	0.384 ± 0.006	0.006	NBF-selected	–	1	...	$-1.7^{+0.14}_{-0.21}$
Glazebrook et al. (2004)[Hβ]	0.458 ± 0.099	”	”	–	1	...	$-1.04^{+0.17}_{-0.14}$
Pascual et al. (2001)	$0.228 < z < 0.255$	0.19	NBF Hα-selected	52	1.4	...	$-1.3138^{+0.08}_{-0.07}$
Hayes, Schaerer & Östlin (2010)	$2.214 < z < 2.246$	0.016	NBF Hα-selected	55	1	...	-0.74 ± 0.2
+ Geach et al. (2008)	$2.214 < z < 2.246$	0.6	NBF Hα-selected	55			
James et al. (2008)	$0 < z < 0.01$	...	Hα imaging	∼330	1	...	-1.72 ± 0.08
Karachentsev & Kaisin (2010)	within 10 Mpc	0.002	Hα imaging	52	1	...	-1.72 ± 0.06
Tadaki et al. (2011)	$2.214 < z < 2.246$	∼0.016	NBF Hα-selected	66	1	...	-0.51
Pascual (2005)[j]	∼0.24						$-1.39^{+0.3}_{-0.3}$
	∼0.4						$-1.26^{+0.4}_{-0.2}$
Doherty et al. (2006)	$0.77 < z < 1.0$	0.026	Hα survey using CIRPASS[k]	38	1	...	-1.13 ± 0.1
Pettini et al. (1998)[i]	$2 < z < 3.5$	...	Near-IR selected	5	0.784	...	-0.557 ± 0.15

[a]Hα-selected surveys use either slitless spectroscopy (SLS), or narrow-band filters (NBF).
[b]Number of galaxies.
[c]The factor used in converting $\dot{\rho}_*$ from the cosmology assumed in the original reference to the cosmology assumed here. Equation 1 in Hopkins (2004) is used to obtain the conversion factor.
[d]The original reference only reports an observed $\dot{\rho}_*$, the value given here is cosmology/IMF corrected. IMF used is Salpeter.
[e]The final value converted to our assumed cosmology, and (Salpeter) IMF. Even though we assumed a Baldry & Glazebrook (2003) IMF for the analysis presented in the main paper, the SFR density measurements presented in this table and in Table B2 are based on a Salpeter (1955) IMF as many of the SFR density measurements in the literature are based on Kennicutt (1998) relation that assume a Salpeter (1955) IMF. To change the IMFs from Salpeter (1955) (used to estimate the SFR densities in Tables B1 and B2) to Baldry & Glazebrook (2003) (used in the main paper) simply add -0.43 to log $\dot{\rho}_{*,int}$ measurements.
If the quoted SFR density measurement in the original reference is uncorrected for dust obscurations, a corrected based on the assumption of a one magnitude extinction in Hα (Hopkins & Beacom 2006) is applied to log $\dot{\rho}_{*,int}$ measurements presented above.
All SFR density values reported here are log $\dot{\rho}_*(L > 0)$. If the original reference reports an SFR density above a limiting flux, then it is indicated here within the parentheses underneath.
[f]Optically selected and morphology-classified bright galaxies from the SDSS northern stripe.
[g]The SFRD value reported here is from Ly et al. (2011).
[h]Estimates of cosmic (sample) variance is included in the uncertainties.
[i]Measurements from Hopkins (2004).
[j]Measurement taken from Villar et al. (2008).
[k]Near-IR multi-object spectograph Cambridge Infrared Panoramic Survey Spectograph on the William Herschel Telescope.

Table B2. Compilation of [O II] λ3727 and [O III] λ5007 emission-line SFRD measurements.

Reference	Indicator	Redshift (z) (z)	Selection	N	C_1	log $\dot{\rho}_{*,\mathrm{obs}}$ ($M_\odot$ yr^{-1} Mpc^{-3})	log $\dot{\rho}_{*,\mathrm{int}}$ ($M_\odot$ yr^{-1} Mpc^{-3})
Sullivan et al. (2000)	[O II] λ3727	$0 < z < 0.3$	UV-selected, FOCA	∼216	0.55	...	-1.64 ± 0.06
Hippelein et al. (2003)	[O II] λ3727	$0.866 < z < 0.894$	NBF Hα-selected	∼222(total detected)	1.00	...	$-1.00^{+0.12}_{-0.17}$
	[O II] λ3727	$1.175 < z < 1.211$	”	”	1.00	...	$-0.68^{+0.09}_{-0.12}$
	[O III] λ5007	$0.39 < z < 0.412$	”	∼124(total detected)	1.00	...	$-1.33^{+0.13}_{-0.18}$
	[O III] λ5007	$0.626 < z < 0.646$	”	”	1.00	...	$-1.61^{+0.09}_{-0.11}$
Gallego et al. (2002)	[O II] λ3727	$0 < z < 0.05$	SLS Hα-selected, UCM	191	0.67	-3.02 ± 0.15	-2.03 ± 0.11
Ly et al. (2007)	[O II] λ3727	$0.877 < z < 0.905$	NBF Hα-selected	673	1.00	...	-1.26
	[O II] λ3727	$0.902 < z < 0.922$	”	818	1.00	...	-0.97
	[O II] λ3727	$1.171 < z < 1.203$	”	894	1.00	...	-0.82
	[O II] λ3727	$1.450 < z < 1.485$	”	951	1.00	...	-0.55
	[O III] λ5007	$0.391 < z < 0.431$	”	351	1.00	...	-1.87
	[O III] λ5007	$0.416 < z < 0.444$	”	209	1.00	...	-2.03
	[O III] λ5007	$0.616 < z < 0.656$	”	293	1.00	...	-1.66
	[O III] λ5007	$0.823 < z < 0.868$	”	662	1.00	...	-1.30
Hogg et al. (1998)	[O II] λ3727	$0.1 < z < 0.3$	*R*-selected, CFGRS	375(total)	0.625	...	$-1.865^{+0.101}_{-0.094}$
	[O II] λ3727	$0.2 < z < 0.4$	”	”	0.601	...	$-1.925^{+0.163}_{-0.118}$
	[O II] λ3727	$0.3 < z < 0.5$	”	”	0.583	...	$-1.271^{+0.105}_{-0.085}$
	[O II] λ3727	$0.4 < z < 0.6$	”	”	0.570	...	$-1.020^{+0.075}_{-0.067}$
	[O II] λ3727	$0.5 < z < 0.7$	”	”	0.559	...	$-1.188^{+0.072}_{-0.062}$
	[O II] λ3727	$0.6 < z < 0.8$	”	”	0.552	...	$-1.272^{+0.088}_{-0.073}$
	[O II] λ3727	$0.7 < z < 0.9$	”	”	0.547	...	$-1.247^{+0.081}_{-0.071}$
	[O II] λ3727	$0.8 < z < 1.00$	”	”	0.543	...	$-1.146^{+0.090}_{-0.074}$
	[O II] λ3727	$0.9 < z < 1.10$	”	”	0.540	...	$-0.941^{+0.107}_{-0.087}$
	[O II] λ3727	$1.00 < z < 1.20$	”	”	0.539	...	$-1.046^{+0.199}_{-0.136}$
	[O II] λ3727	$1.10 < z < 1.30$	”	”	0.538	...	$-1.066^{+0.301}_{-0.176}$
Takahashi et al. (2007)	[O II] λ3727	$1.17 < z < 1.20$	NBF, [O II] λ3727-selected, *HST* COSMOS	3176	1.00	...	$-0.495^{+0.075}_{-0.058}$
	[O II] λ3727	$1.17 < z < 1.20$	NBF, [O II] λ3727-selected, SDF	294	1.00	...	$-0.854^{+0.216}_{-0.105}$
Teplitz et al. (2003)	[O II] λ3727	$0.46 < z < 1.415$	SLS, [O II] λ3727-selected, *HST* STIS	71	1.00	-1.55 ± 0.06	-1.005 ± 0.11
Hammer et al. (1997)	[O II] λ3727	$0.25 < z < 0.5$	*I*-selected, CFRS	∼212(total sample)	1.04	$-2.20^{+0.070}_{-0.080}$	$-1.705^{+0.070}_{-0.080}$
	[O II] λ3727	$0.5 < z < 0.55$	”	”	0.95	$-1.72^{+0.11}_{-0.15}$	$-1.226^{+0.11}_{-0.15}$
	[O II] λ3727	$0.55 < z < 1.00$	”	”	0.892	$-1.35^{+0.20}_{-0.38}$	$-0.855^{+0.20}_{-0.38}$
Bayliss et al. (2011)	[O II] λ3727	$1.822 < z < 1.878$	NBF, [O II] λ3727-selected, HAWK-I VLT	26	1.00		$-0.42^{+0.064}_{-0.075}$
Sobral et al. (2012)	[O II] ∼ λ3727	$1.45 < z < 1.49$	NBF, HiZELS	1379	1	...	$-0.770^{+0.09}_{-0.12}$ (assuming $A_{\mathrm{H}\alpha} = 1$ mag)
							$-0.62^{+0.097}_{-0.12}$ (Independent estimate)

star-forming galaxies. Fig. A3 shows the distribution of luminosities in four redshift bins compared to the distribution of luminosities of objects classified as composites based on the Kauffmann et al. (2003) relation. The lowest redshift ($z < 0.1$) sample consists of relatively small number of composites, and this number increase with redshift. A number of studies (e.g. Best et al. 2005; Xue et al. 2010) have found that the AGN fraction increases with the stellar mass. Hopkins et al. (2013) show the BPT diagnostics for the GAMA galaxy sample as a function of both redshift and stellar mass, demonstrating the increase in AGN fraction with stellar mass.

The effects of AGN contamination on the lowest ($z < 0.1$) and highest ($0.24 < z < 0.34$) GAMA LFs presented in Section 4.2 are shown in Fig. A4. The effects on $z < 0.1$ Hα LF and the respective SFRD is negligible. Even though the highest-z LF constructed by removing these composites indicate a small drop in number density, the difference that makes to the integrated SFRD is less than 10 per cent.

APPENDIX B: COMPILATION OF SFRDs FROM THE LITERATURE

In Section 6, we present measurements of the SFRD as a function of redshift. Here, we tabulate the measurements from the literature that are shown in Fig. 15, detailing the survey type, area, selection methods if appropriate and various corrections, following the approach of Hopkins (2004). Note that the SFRDs given in this table assume a Sapeter IMF. In order to convert these values to those presented in Fig. 15, simply add a factor of -0.43 to log $\dot{\rho}_{*,\mathrm{int}}$ measurements.

This paper has been typeset from a TEX/LATEX file prepared by the author.